



**THE UNIVERSITY  
OF QUEENSLAND**

A U S T R A L I A

**Recyclable and Biodegradable Glider Airframes for  
Disposable UAVs**

By

*Nicholas Hourigan, 42652605*

School of Information Technology and Electrical Engineering,  
University of Queensland.

Submitted for the degree of  
Bachelor of Engineering Honours  
Extended Major in Mechatronics Engineering

10<sup>th</sup> November 2014



Nicholas Hourigan

119 Brookwater Drive

Brookwater

Queensland 4300

10<sup>th</sup> November 2014

Prof Paul Strooper  
Head of School  
School of Information Technology and Electrical Engineering  
The University of Queensland  
St Lucia QLD 4072

Dear Professor Strooper,

In accordance with the requirement of the Degree of Bachelor of Engineering Honours in the division of Mechatronics Engineering in the School of Information Technology and Electrical Engineering, I submit the following thesis entitled

“Recyclable and Biodegradable Glider Airframes for Disposable UAVs”

The thesis was performed under the supervisor of Dr. Paul Pounds. I declare that the work submitted in thesis is my own, except as acknowledge in the text and footnotes, and has not been previously submitted for a degree at the University of Queensland or any other institution.

Yours sincerely

---

Nicholas Hourigan



## **Acknowledgments**

Firstly, I would like express my gratitude to my supervisor Dr. Paul Pounds for accepting me as the student to undertake this interesting project, but for also providing insight and assistance at the weekly and impromptu meetings.

I would also like to thank Timothy Filmer for his advice and assistance throughout this project. I would specifically like to thank him for his assistance with the meteorological data that was used in the MATLAB simulation.

Additionally, I would like to thank Joshua Collins for letting me use his 3D printer to rapidly prototype the designs for the initial moulds.

Finally, I would like to thank my family for their unwavering support throughout this project. A special thanks goes towards my brother - Christopher Hourigan who supported and assisted me whenever asked; and let me use his 3D printer to print the larger moulds.

## Abstract

There is currently a lack of emphasis on biodegradable airframes that can be used in disposable Unmanned Aerial Vehicles (UAVs). The aim of this project was to design a UAV glider airframe that was made from cardboard based biodegradable and recyclable material. The airframe was also required to be simple to manufacture and achieve an ideal glide slope of 40:1 so that it could be used in a test flight from Sydney to Brisbane through a high altitude weather balloon launch. This project was broken into four subsections, the materials section, mould design section, airfoil selection section and the airframe design section.

The material properties of moulded fibre were found through cantilever beam bending experimentation on moulded pulp beams. It was found that the material had a density of  $413.73 \text{ kg/m}^3$ , a shrinkage of 5.89 %, a maximum allowable strain of 3% and a yield strength of 0.663 MPa [1].

Based on the understanding of the material properties from the beam bending experimentation, moulds were designed and produced which were able to successfully create airframes that utilized accurate airfoils. These moulds utilised a pressure moulding technique which would compress the moulded fibre slurry into the desired shape whilst expelling excess water.

The AG19 Mark Drela airfoil [2] selected had a glideslope of 36.3 at a Reynolds number of 50000. Although this was below the design consideration of a 40:1 glideslope, the trade-off for a smoother pressure distribution was deemed an appropriate compromise. The Reynolds numbers that the aircraft would encounter ranged from 10883 to 53087 based upon MATLAB simulation. At these extremely low Reynolds numbers, the airflow is viscous, and therefore a smooth pressure distribution was necessary to avoid early flow separation.

Based upon the MATLAB simulation a wing span of 400mm and a chord length of 100mm were chosen resulting in a simulated flight distance of 384945m. This was approximately half the distance required to achieve the idealistic design goal of flying from Sydney to Brisbane. Exceeding a 400mm span would increase the difficulty of the manufacturing process; however breaching a primary design goal.

A final airframe was designed in XFLR5 that was inherently stable in all eight stability modes in viscous flow testing. The design utilized a combination of stability enhancing features which reduced the maximum glideslope to 11.2 at an angle of attack of  $10^\circ$ .

## Table of Contents

Acknowledgments .....	v
Abstract .....	vi
List of Figures.....	ix
List of Tables.....	x
1.0 Introduction .....	1
1.1 Basis for Thesis .....	1
1.2 Statement of Intent .....	1
1.3 Key Design Consideration.....	1
1.4 Project Scope .....	2
2.0 Background.....	3
2.1 Previous Work .....	3
2.1.1 Weather Balloon Launch System .....	3
2.1.2 Current disposable UAVs .....	3
2.1.3 Airfoils specifically designed for extremely Low Reynolds Number Airfoils.....	4
2.1.4 Aerodynamic Measurements at Low Reynolds Numbers .....	4
2.1.5 – Moulded Fibre as a Packaging Material .....	5
2.2 Aerodynamics.....	6
2.2.1 Lift .....	6
2.2.2 Drag .....	6
2.2.3 Glide Slope .....	7
2.2.4 Aspect Ratio .....	8
2.2.5 Reynolds Number .....	8
2.2.6 Control.....	9
2.2.8 Stability.....	10
3.0 Understanding Moulded Pulp.....	12
3.1 Methodology.....	12
3.2 Beam Manufacturing .....	12
3.3 Moulded Fibre Beam Testing .....	14
3.4 Material Results and Discussion.....	16
4.0 Mould Design .....	18
4.1 Mould Design Iterations .....	18
4.1.1 Nano Plane Mould .....	18
4.1.2 Beam Mould #1 .....	19
4.1.3 Beam Mould #2 .....	20
4.1.4 Limitations Test Mould .....	21
4.1.5 Final Mould .....	24

5.0 Airfoil Selection .....	28
5.1 Airfoil Selection Methodology .....	28
5.2 Airfoil Simulation and Results .....	29
6.0 Airframe Design .....	30
6.1 Airframe Design Methodology.....	30
6.2 Chord Length and Span Results and Discussion .....	31
6.3 Stability Design Results and Discussion .....	33
7.0 Conclusion .....	36
Appendix A .....	38
Appendix B.....	39
Appendix C.....	41
Appendix D .....	42
Appendix E.....	46
Appendix F .....	55
Appendix G .....	57
Appendix H .....	59
Appendix I.....	62
Appendix J.....	63
Appendix K .....	64
Appendix H .....	65
Bibliography .....	66

## List of Figures

Figure 1 - Glideslope Vs Reynolds Number [10] .....	5
Figure 2 - Aspect Ratio [14] .....	8
Figure 3- Six Degrees of Freedom.....	10
Figure 4 - Beam Mould #2 .....	12
Figure 5 - Steps 1-4 of producing moulded fibre beams.....	13
Figure 6 – Steps 5-8 of producing moulded fibre beams .....	13
Figure 7 - Beam 2 No Load .....	15
Figure 8 - Beam 2 800 gram Load .....	15
Figure 9 - Beam 2 Failure at 900 grams.....	15
Figure 10 - Beams 1-9 after failure .....	16
Figure 11 - Cantilever Beam Bending Results.....	17
Figure 12 - Nano Plane Mould.....	19
Figure 13 - Beam Mould #1 .....	20
Figure 14 - Beam Mould #2 .....	20
Figure 15 - Mould Design Process for Airfoils.....	21
Figure 16 - Limitations Test Mould.....	22
Figure 17 - Sample 3 from Limitations Test Mould .....	23
Figure 18 - Closeup of surface finish from sample 3.....	24
Figure 19 – CES 2014 Mould Material Selection Chart.....	25
Figure 20 - Final Mould Bottom .....	27
Figure 21- Final Mould Top.....	27
Figure 22 - Modified AG19 Reflex Airfoil from assembled final mould.....	27
Figure 23 - planeSim.m plots .....	33
Figure 24 - Final Airframe Design in XFLR5 .....	34

## **List of Tables**

Table 1- Beam Dimensions after curing .....	14
Table 2 - Manufactured Prototypes from Limitations Mould.....	23
Table 3 - Comparison of Materials for Mould .....	25
Table 4 – Table of candidate Airfoils .....	29
Table 5 - Results from Varying Chord and Span.....	32

## **1.0 Introduction**

### **1.1 Basis for Thesis**

There are currently few Unmanned Aerial Vehicles (UAVs) that exist which are designed for a single, disposable use. These UAVs typically utilise materials such as non-biodegradable foams and plastics to manufacture the airframes which when left behind in the environment can cause detrimental effects to the surroundings. Disposable UAVs allow for sensors and other payloads to be deployed into areas and situations that are often difficult or expensive to reach, such as the arctic or deep rain forest. To keep these environments pristine it is imperative that any disposable UAV that may be deployed into these locations causes minimal impact to the surroundings.

### **1.2 Statement of Intent**

This thesis aims to investigate the use of recyclable and biodegradable in the production of a long range UAV glider airframe. The airframe is to be designed for a high altitude launch from approximately 30000 metres via a weather balloon. The idealistic design goal for this airframe is to glide the distance from Sydney to Brisbane; approximately 730000 metres [3]. For this to be achieved it is expected that the aircraft would be fitted with a control and guidance system so that the aircraft can stay on the intended flight path. However to reduce the dependency on these systems, the airframe will be designed to be intrinsically stable to minimize the input and therefore power consumption of the control system.

### **1.3 Key Design Consideration**

The focus of this project is on the biodegradable nature of the airframe; which provided the biggest project constraint – the material. In this case, the material that is to be used is moulded fibre, or moulded pulp which is a cardboard based material. Based upon this constraint and the idealistic design goal of a 730000 meter glide from an initial altitude of 30000 metres, the following key considerations were made:

- The airframe must be manufactured from a recycled cardboard moulded fibre technique
- The airfoil must achieve a glideslope of 40:1
- Design the airframe so that it is inherently stable.
- The airframe must be extremely low cost and simple to manufacture after the mould is produced.

## **1.4 Project Scope**

The purpose of this thesis is to design only the glider airframe. The goal of this airframe is for it to be used in other projects that would focus on either the navigation or control of the airframe. This project is also limited to a budget of \$250 AUD.

## **2.0 Background**

The use of recyclable materials to create a single use UAV or MAV is relatively novel. Before this can be pursued an understanding is required in the fields of aerodynamics, aircraft design and moulded fibre manufacturing.

### **2.1 Previous Work**

#### **2.1.1 Weather Balloon Launch System**

Although this project does not include the design of the launch system, it was important to know the capable altitudes ranges of the proposed weather balloon launch system. The highest launched StratoStar weather balloon was launched by DePauw University in Illinois which reached a maximum altitude of 38 kilometres [4].

A project led by David Windestål utilized a weather balloon for a project with a similar goal [5]. The goal of this project was to launch a glider to the edge of space, release it and glide it to the starting position using a First Person View (FPV) setup. The glider launched at an altitude of approximately 30 kilometres and did not reach the intended starting position due to technical difficulties with the FPV system. Due to the altitude, research indicated that the glider needed to endure extreme temperatures as low as -50°C which had the potential to cripple the on board electronics and actuators. Therefore the electronic components were modified to be able withstand these harsh conditions. The control surfaces on the airframe were actuated via servos which had the lubricants removed to prevent the gears from binding as the viscosity of the grease increased with decreasing temperature. The glider landed approximate 101 kilometres away from the intended final destination; partially due to the technical difficulties but also due to the velocities of the high altitude winds [5]. The data collected from this research shows how the effects of the high altitude wind can easily overpower the control of the glider as the gliders final destination was 101km from its starting point.

#### **2.1.2 Current disposable UAVs**

The disposable paper plane designed by Dr. Paul Pounds was designed for the intention of low cost remote destination sensor deployment [6]. Due to the paper based nature of this design, the airframe would degrade into the environment after the mission was completed. A single piece of standard A4 paper was used to design the airframe, resulting in a small payload capability. The airframe was controlled by voice coil actuators which actuate the control surface based on a voltage input. The need for no lubricants negates the possibilities of the control surfaces binding at extremely low temperatures.

The University of Sheffield designed a disposable UAV from Fuse Deposition Modelling (FDM) 3D printing [7]. The material utilised for the airframe was ABS plastic which is not biodegradable; although had more ideal mechanical properties compared to paper or cardboard. Therefore this allowed for a 1.5 metre wingspan which is what would be required for long range gliding.

The University of Colorado created the DataHawk in order to deploy a thermodynamic sensor package over fields of interest, such as the Arctic Ocean [8]. The airframe utilised was constructed from polypropylene foam, another non-biodegradable material. Rather than utilising a high altitude weather balloon for launch, the DataHawk utilises a motor and propeller so that it can guide itself to the pre-determined destination. As a result the DataHawk is relatively expensive, costing in the neighbourhood of \$600.

Based on these systems it is apparent that a gap exists for a biodegradable based UAV that could carry decent payloads; in the range of 20 to 100 grams.

### **2.1.3 Airfoils specifically designed for extremely Low Reynolds Number Airfoils**

The thesis by Michael Reid investigated the use of Bezier curves to create airfoils targeted at extremely low Reynolds numbers. The aim of the thesis was to determine a relationship between thin/cambered/reflexed airfoil performance and airfoil shape parameters to improve future airfoil designs at low Reynolds numbers. XFOIL, a two dimensional analysis program designed by Mark Drela specifically for the analysis of airfoils at low Reynolds numbers was used to test these Bezier curve airfoils. The results from XFOIL were tested against wind tunnel results and showed good correlation for airfoils with camber less than 7% [9]. These airfoils will need to be tested, and possibly used in the airframe.

### **2.1.4 Aerodynamic Measurements at Low Reynolds Numbers**

The research presented by Thomas J. Mueller explores the complex issues of flow at low Reynolds numbers in order to design the most efficient, stable and controllable MAV [10]. Figure 1 portrays the importance of Reynolds number of maximum section glide slope. The report indicates that for Reynolds numbers in the range of 10000 to 30000 the boundary layer is completely laminar; therefore once the layer separates and causes stall, it does not reattach and the plane cannot recover. Between the range of 30000 to 70000 airfoils with a thickness greater than 6% can cause hysteresis effects caused by laminar flow separation with transition to turbulent flow. Therefore it is suggested to use thinner airfoils in this Reynolds number region.

Many airfoils were tested and it was found in low Reynolds number wind tunnel testing that cambered wings performed better than flat plate wings due to their better aerodynamic properties. Although the drag increased the glide ratio was improved over flat plate wings as the lift was

considerably improved. The effect of trailing edge geometry was also tested and it was found that tapered trailing edges at low aspect ratios would produce a slightly positive moment coefficient while elliptical trailing edges would produce slightly negative moment coefficient.

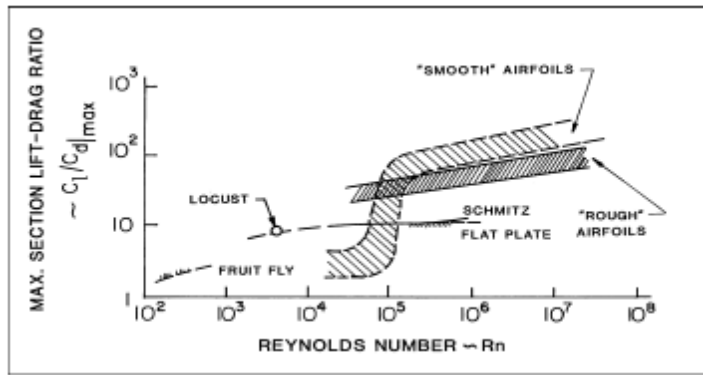


FIGURE 1 - GLIDESLOPE VS REYNOLDS NUMBER [10]

### 2.1.5 – Moulded Fibre as a Packaging Material

Moulded fibre (or moulded pulp) has traditionally been used as a recyclable and biodegradable packaging for many products such as egg cartons. Moulded fibre techniques can utilise many different fibre material compounds however it is typically produced entirely from recycled cardboard which is then combined with water and mixed into a slurry. Currently, three primary methods are used to process moulded fibre however these are for high unit production runs using vacuum forming technology quickly produce the required product [11]. Although vacuum technology was not used in this project the data acquired from these production methods can provide an indication of what is practically possible with the material. Moulded pulp performs similarly to polymer based expanded polystyrene (EPS) at certain static loadings [12]. EPS is a common material used in model airframes, suggesting that cardboard moulded fibre may be suitable.

Research by the Nanjing University of Technology was conducted with regards to using various plant fibre mixes with cardboard and newspaper to form moulded fibre fruit trays. Appendix A displays the results from testing the compression resistance and cushioning properties of the materials. These results indicated that corrugated cardboard box pulp had the best performance in regards to the testing that was performed [13]. Although more testing is required to find the mechanical properties of the cardboard moulded fibre, this material can be used as a starting point for testing and design.

The thesis paper *Packaging Systems Redesign: A Study in Designing More Sustainable Product Packaging Systems* [1] covers in detail the mechanical properties of various samples of moulded

pulp through various tests from high precision instruments such as the Instron 5869. Correlation between these results and those found through testing may be valuable to save time and resources.

## 2.2 Aerodynamics

### 2.2.1 Lift

In its most simplistic terms, lift is generated by producing a higher pressure under a wing and a lower pressure above the wing. The pressure is generated by the wing when the angle of attack relative to the oncoming flow of air is greater than the zero lift angle of the airfoil. Subsequently increasing the angle of attack will increase the amount of lift produced until a stalling point is reached, at which the drag produced exceeds the lift force or flow separation occurs. The lift force acts through the centre of lift which is not a static position on the airframe. As the angle of attack increases on a cambered wing, the centre of lift shifts forward. The amount of lift produced by a wing can be calculated using:

$$L = \frac{1}{2} \rho V^2 A C_L \quad (1)$$

Where  $L$  is the lift force,  $\rho$  is the density of air,  $V$  is the velocity of the air relative to the wing,  $A$  is the area of the wing plan and  $C_L$  represents the lift coefficient which is based on the wing geometry [14]. In gliding flight the lift produced is equals to the mass of the aircraft multiplied by gravity. Although this seems simple there are many other factors involved that influence lift rather than just the pressure difference on opposite sides of the wing. Concepts such as conical vortex lift are important to understand however its use for this project is limited as it results in a poor lift to drag ratio with straight, unswept wings that are often deployed on long range gliding aircraft. Although the use of this concept is limited by the scope of the project, it serves as an important basis to understanding the importance that the wing bound vortex, trailing vortex (induced drag) and starting vortex have in producing lift [14].

### 2.2.2 Drag

The drag of an aircraft can be calculated based on two main forces; a component of force due to the pressure distribution from the aircraft surfaces, and the force caused by viscous shearing [14]. Therefore an equation can be formed to calculate the drag of an airframe or airfoil:

$$D = \frac{1}{2} \rho V^2 A C_D \quad (2)$$

Where  $D$  is the drag force and  $C_D$  is the drag coefficient. This can be expressed as a parabolic drag polar which is comprised of the parasitic drag coefficient ( $C_{D_0} = \text{skin friction} + \text{form drag}$ ) and the induced drag coefficient ( $K = (\pi * \text{Aspect Ratio} * \text{efficiency factor})^{-1}$ ) [15] [16]:

$$C_D = C_{D_0} + KC_L^2 \quad (3)$$

Therefore it is apparent that the induced drag directly correlates to the aspect ratio of the plane; the larger the aspect ratio the lower the induced drag. The parasitic drag coefficient is based on the airfoil profile and surface finish where the thinner the airfoil the less form drag is produced [17]. An airspeed exists where the induced drag and form drag are at a minimum which is the ideal velocity for the aircraft to fly at to maximise glide slope; the equation for this minimum drag airspeed is:

$$V_{md} = \left( \frac{K}{C_{D_0}} \right)^{\frac{1}{4}} \sqrt{\frac{2mg}{\rho A}} \quad (4)$$

Where  $V_{md}$  the minimum is drag airspeed,  $m$  is the mass and  $g$  is gravity.

### 2.2.3 Glide Slope

Gliders are highly efficient aircraft that usually require an external source of lift or thrust to provide the initial altitude required. In ideal conditions, the gliders altitude decreases at a constant rate of the glide slope which is the lift to drag ratio based on a certain angle of attack [18].

It is of utmost importance that the design of the glider maximises the glide slope. The maximum glide slope remains relatively constant irrespective of wing load or weight. However as a result of increasing the weight of the glider the maximum glide slope occurs at a higher relative air speed. Although modern sailplanes and gliders can achieve maximum glide slopes of 60:1, a review of 104 model sailplanes with the same aerofoil but varying aspect ratios found the maximum glideslope of a model aircraft to be 25:1 [20]. It must also be noted that these models were not limited in design to a single recyclable material.

Consequently it may not be possible to achieve a glide slop of 40:1 in this project, however it will be attempted. Knowing this it is therefore vital that the glide slope is maximised. This can be implemented by designing a wing with a high aspect ratio.

The rate at which the aircraft sinks can be calculated using the following formula where  $\dot{h}$  is the sink rate:

$$\dot{h} = - \sqrt{\frac{mg}{1/2\rho A} \frac{C_D}{C_L^{1.5}}} \quad (5)$$

## 2.2.4 Aspect Ratio

The aspect ratio is defined as the ratio of the overall wing span to the average chord.

$$AR = \frac{S}{C} = \frac{S^2}{A} \quad (6)$$

Where  $AR$  is the aspect ratio,  $S$  is the wing span and  $C$  is the mean chord. High aspect ratios provide high ratio glide slopes and are therefore used on long range aircraft. This is because high aspect ratio wings with short chord lengths are required to create long, weak bound vortices over the surface of the wing. In doing so, the trailing vortices that form behind the wing induce less drag. This closed wing vortex system provides efficient lift at low speeds which is ideal for gliders [14].

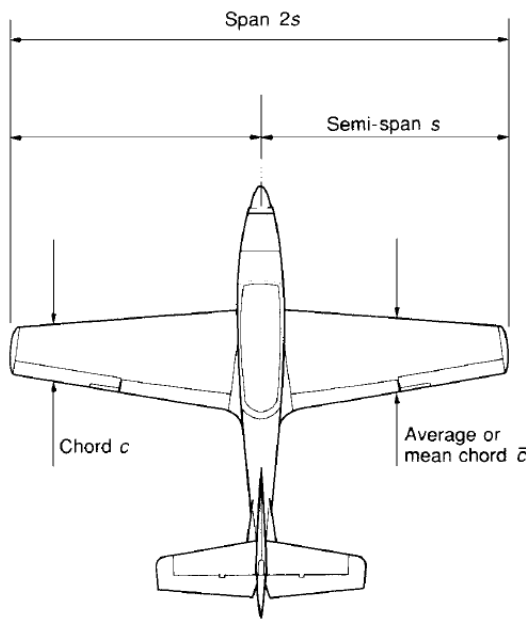


FIGURE 2 - ASPECT RATIO [14]

## 2.2.5 Reynolds Number

As an aircraft passes through air, the air molecules stick to the surface of it. This creates the boundary layer – a layer of air near the surface of the aircraft which effectively changes the shape of the aircraft. The edge of this layer reacts to the air as if it were a physical surface, however it is possible that the boundary layer may separate from the object. This can create an effective shape

that varies greatly from the physical shape behind it. This can significantly alter the drag characteristics of the aircraft [14].

As the type of boundary layer influences surface friction drag and flow separation it is important to understand what factors control the transition from laminar to turbulent boundary layer flow. The transition position of turbulent flow moves forward with increasing velocity and air density. This position moves aft if the coefficient of viscosity is increased. Therefore the relationship between transition position and the aforementioned factors is known as the Reynolds number.

$$Re = \frac{\rho V C}{\mu} \quad (7)$$

Where  $\mu$  is the viscosity coefficient. Reynolds numbers in the order of 10 million indicate that viscous forces are so minute that the flow is essentially inviscid. Low Reynolds numbers, in the order of 100 indicate that viscous forces definitely need to be considered. Although this number is dimensionless, it represents the ratio of inertial forces to viscous forces [21]. It also represents the type of flow that can be expected from a certain wing profile – a critical component of aerofoil design.

Typical full scale sailplane gliders operate in the Reynolds number region of approximately 60000 to 300000 [22]. In small scale, MAV's typically operate in Reynolds number between 30000 to 70000 [10] although this project may see Reynolds Numbers as low as 10000 due to the high altitude launch resulting in extremely low densities and viscosity coefficients. At Reynolds numbers this low the flow is completely laminar; if flow separation occurs the layers will not reattach causing stall [10]. In regions of laminar flow, the boundary layer can only handle graduate changes in pressure [22]. Therefore it is important to choose an airfoil with a smooth pressure distribution.

## 2.2.6 Control

The six degrees of freedom that aircraft possess are:

- Roll rotation
- Pitch rotation
- Yaw rotation
- Axial translation
- Transverse translation
- Normal translation

Basic model aircraft do not require translational control, and are often flown on the basis on roll, pitch and yaw control. This requires ailerons, elevators and rudders for the corresponding control

surfaces. More control surfaces such as flaps and trim tabs are often used on larger aircraft but this is out of scope for the project and would unnecessarily increase the complexity for little gain. The flying wing airframe would be controlled by elevons at the rear of the aircraft to allow for roll and pitch rotational control to keep the aircraft on the correct flight path.

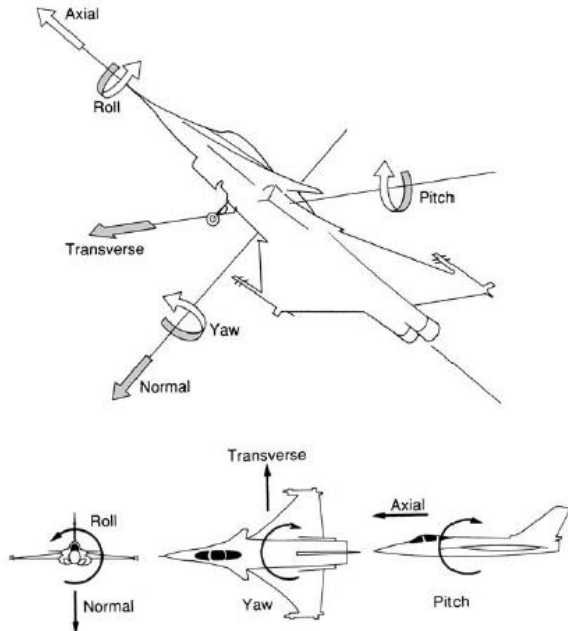


FIGURE 3- SIX DEGREES OF FREEDOM

### 2.2.8 Stability

The stability on an aircraft can be divided into two sections; static and dynamic stability. For an aircraft to be statically stable it must return to its prior flight conditions after an impulse force has been applied. This has to be completed through the production of forces and moments created by the design of the aircraft [14]. In a flying wing there is no lift force from the tail section to counteract the lift from the main wing, so the position of the centre of gravity may need to be altered to ensure that the forces balance.

An aircraft is defined as dynamically stable if the oscillatory motion of the aircraft is negated over time after an impulse. The speed at which the aircraft returns to its original flight path is dependent on the amount of damping. An aircraft can be statically stable and dynamically unstable simultaneously if the corrections made to the oscillations keep increasing; this is known as negative damping [14].

A total of eight stability modes need to be tested. The longitudinal stability modes are comprised of two symmetric phugoid modes and two symmetric short period modes [23]. The lateral stability modes are comprised of one spiral mode, one roll damping mode and two Dutch roll modes [23].

Producing a statically and dynamically stable airframe is critical to ensure that minimalistic control is required to govern the aircraft; requiring less energy storage and therefore mass on the aircraft. Dynamic stability of the proposed airframe could be achieved by utilizing dihedral and wing sweep to achieve lateral stability; twist and reflexed airfoils to achieve longitudinal stability [23]. Another factor that is critical in ensuring that the airframe is stable is to position the centre of gravity in front of the neutral point if a flying wing is used.

### 3.0 Understanding Moulded Pulp

Before an airframe could be designed it was required to explore the material properties of moulded fibre to understand the design limits that would be enforced on the airframe.

#### 3.1 Methodology

It was decided to perform cantilever beam bending experimentation on formed moulded fibre samples in order to extract key material properties. Cantilever beam bending was used as it would provide the necessary material data, but also demonstrate the failure mode that could occur with excessive wing loading.

The following equations were used to calculate the material properties with the assumption of small angle approximation and a small plastic deformation region [23].

$$E = \frac{\sigma}{\epsilon} \quad (8)$$

Where  $E$  is the Young's modulus,  $\sigma$  is the stress,  $\epsilon$  is the strain

$$I = \frac{bh^3}{12} \quad (9)$$

Where  $I$  is the second moment of area,  $b$  is the width of the beam and  $h$  is the height of the beam.

$$\sigma = -\frac{My}{I} \quad (10)$$

Where  $\sigma$  is the stress and  $M$  is the moment force and

#### 3.2 Beam Manufacturing

Before the cantilever beam bending experimentation could be conducted it was required that moulded fibre beams were produced of a known dimension prior to testing. The beams were produced using a 3D printed mould (Beam Mould #2) from ABS plastic which had internal dimensions of 120mm × 15mm × 15mm.



FIGURE 4 - BEAM MOULD #2

The process used to manufacture these moulded fibre beams was:

1. Break down existing moulded fibre products to a pulp with hot water and a blender. Blend until consistent.
2. Extract the moulded fibre slurry from the blender.
3. Remove the excess liquid from the moulded fibre slurry using a sift.
4. Place the material into the Beam Mould #2.
5. Compress the plunger into the mould until the cut-outs are lined up; repeat step 4 if necessary.
6. Force the plunger through the mould to extract the beam.
7. Cure the beam in the oven at 120 °C for 35 minutes.



FIGURE 5 - STEPS 1-4 OF PRODUCING MOULDED FIBRE BEAMS

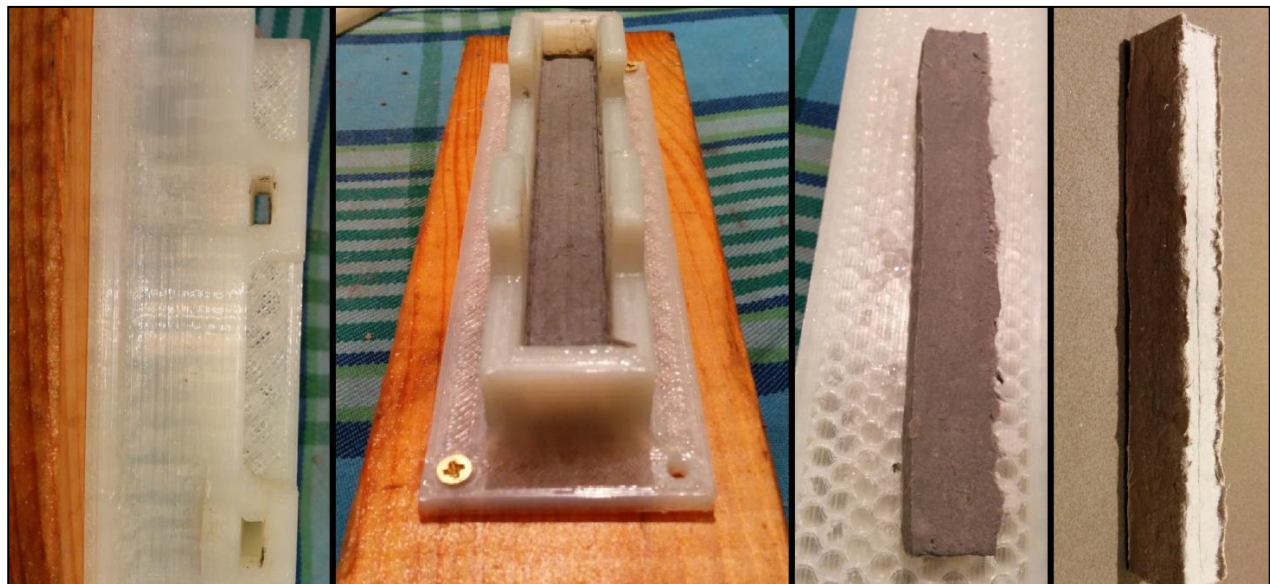


FIGURE 6 – STEPS 5-8 OF PRODUCING MOULDED FIBRE BEAMS

Hot water was used to help loosen the existing bonds and expand the cells of the material so that these could be more easily separated. The temperature of 120 °C was selected as testing done at 165 °C resulted in the core of the beam being uncured whilst the outer faces of the beam were starting to darken and char. Temperatures below 100 °C resulted in long cure times as the water could not successfully turn into vapour to cause the moulded pulp to dry quickly.

A total of nine beams listed in Table 1 were produced using Beam Mould # using this method.

TABLE 1- BEAM DIMENSIONS AFTER CURING

Beam Number	Mass (g)	Length (mm)	Width (mm)	Height (mm)
1	9.9	114.9	13.9	14.1
2	10.5	114.5	13.8	14.2
3	10.6	115.0	13.8	15.0
4	6.4	114.5	13.9	10.2
5	6.8	114.4	13.8	10.3
6	7.3	113.8	14.2	11.5
7	8.5	113.3	14.1	14.1
8	8.9	115.2	14.1	13.8
9	8.2	113.4	14.1	13.8

Beams numbered 1-6 were produced using source material from protective packaging whilst beams numbered 7-9 were produced using egg cartons. A noticeable difference in colour and texture roughness was present between these two raw materials. Beams numbered 4-6 were purposefully designed with less thickness however in the manufacturing of beam 4 a bend was induced into the beam resulting in premature failure; therefore this result was counted as an outlier.

### 3.3 Moulded Fibre Beam Testing

The cantilever beam bending testing was conducted by constraining 20mm of the beam within a vice and applying a load 15mm from the edge of the beam. The load was incremented in 100g intervals until failure and the deflection was measured against the initial no load measurement. Figures X-Y depicts the initial measurement, final measurement and failure points of the testing for Beam 2.



FIGURE 7 - BEAM 2 NO LOAD



FIGURE 8 - BEAM 2 800 GRAM LOAD



FIGURE 9 - BEAM 2 FAILURE AT 900 GRAMS

All nine beams were tested and found to behave similarly, other than Beam 4 due to the induced bend from manufacturing which failed early as a result of a detrimental shape factor. Figure 10 shows all 9 beams tested after failure.



FIGURE 10 - BEAMS 1-9 AFTER FAILURE

As a reference a beam made from 3 layers (13.5mm in height) of foam board was tested as a comparison which can be seen in Appendix B. The foam was layered in the same orientation as to how they would be used on an airframe. This material is commonly used in hobby made airframes due to its low density and high stiffness. The beam did not fail however it had an extremely large plastic deformation region which began much earlier than the moulded fibre beams.

### 3.4 Material Results and Discussion

From the data listed in Table 1 due to the manufacturing of the beams, the following properties were found:

$$\text{Average Density} = 413.73 \text{ kg/m}^3$$

$$\text{Average Shrinkage} = 5.89 \%$$

Raw data for the beam bending experimentation can be found in Appendix B. From analysing the raw data the following material properties were found:

$$\text{Lowest Max Stress} = 1.21 \text{ MPa}$$

$$\text{Lowest Max Strain} = 0.003$$

$$\text{Average Young's Modulus} = 339.37 \text{ MPa}$$

These results correlated with those found in Sample 3 of *Packaging Systems Redesign: A Study in Designing More Sustainable Product Packaging Systems* [1]. Therefore the Yield Strength results for Sample 3 were used in order to save time and resources as opposed to carrying out tensile load experimentation.

$$\text{Yield Strength} = 0.663 \text{ MPa}$$

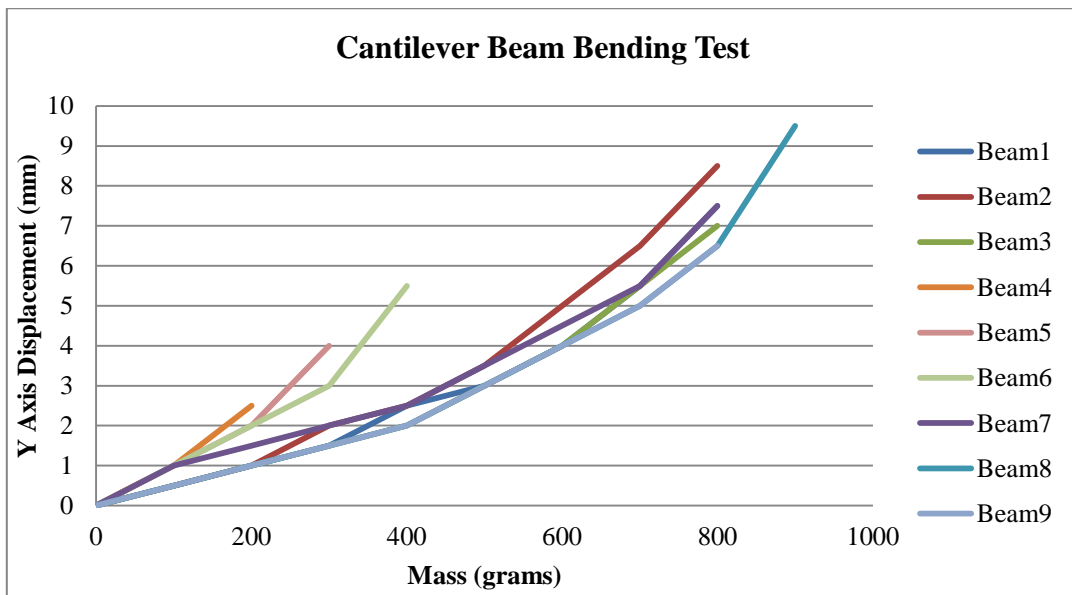


FIGURE 11 - CANTILEVER BEAM BENDING RESULTS

From Figure 11 it was apparent that there was no significant variance in data from using the different sources of moulded fibre. In an effort to reduce parallax error a Nikon D3200 DSLR was setup on a fixed tripod to capture the photos of deflection for each incremental mass; the vice used to secure the beams was also fixed. Measured lines were placed on each beam before testing to ensure consistency in securing and point of loading for each beam. The accuracy of the data could have been increased by using smaller mass increments however due to the nature of the material and manufacturing technique a relatively large safety factor would need to be factored into the final design to ensure unexpected failure does not occur.

The moulding and drying technique used for the beams also varied from the final method used in moulding and drying the airframes due to the shape of the product required. Due to the parallel sides of the mould in Beam Mould #2, material could be compressed to its limits using the plunger before additional material could be added. This was not possible with an airfoil shaped mould as the trailing and leading edges of the mould would contact; limiting the amount of compression possible. Unless the perfect amount of material was used in the final airframe moulds, the density of the airframe would be reduced resulting in less than ideal properties.

## **4.0 Mould Design**

The three moulding methods currently utilised in industry for moulded pulp manufacturing are:

1. Thick/Heavy walled Moulding: 6.35mm – 7.935mm wall thickness. Mould side moderately smooth, opposite side is coarse. Oven drying is needed
2. Transfer Moulding: 1.5875mm – 4.7625mm wall thickness. Mould side and transfer side are relatively smooth. Oven drying is also needed
3. Thermoformed Fibre Moulding: 1.5875mm – 3.175mm wall thickness. Cure in mould technology resulting in high accuracy and smooth parts.

In the manufacturing of these parts a single sided mesh type mould is swept through a vat of moulded fibre slurry. This slurry is then vacuum formed to mesh mould to increase surface finish and remove excess water. This moulding technique produces two surface finishes; the moulded side which is of high quality and the unmoulded side which is rough and appears unfinished. This type of single sided mould would not be able to produce an airframe due to the two sided nature of the design. Although thermoformed fibre moulding uses cure in mould technology which results in both sides of the product being heated; the product is still based off the single mould. The requirement of a vacuum device would also increase the complexity and costs of manufacturing which is against the aims of the project.

### **4.1 Mould Design Iterations**

As the current moulding techniques for moulded fibre are not suitable for this project, a different type of moulding must be selected. This was explored through an iterative design process. A total of 5 moulds were designed and manufactured throughout the timeframe of this project. These moulds were:

1. Nano Plane Mould
2. Beam Mould #1
3. Beam Mould #2
4. Limitations Test Mould
5. Final Mould

#### **4.1.1 Nano Plane Mould**

The aim of the Nano Plane Mould was to test the feasibility of casting of moulded pulp for thicknesses up to 10 mm without vacuum forming. A basic aircraft shape was designed into a mould and 3D printed to minimize the duration mould manufacturing process. When trying to compact the moulded fibre slurry into the mould it was found that mould drainage would play a significant role in the drying time of the casting. This was due to the porous and absorbent nature of

cardboard which would retain significant amounts of water as could be seen in Steps 2 and 3 of Figure 6. It was found that without added heat and airflow this small mould would take over three days to fully dry. As this mould was an initial test, no plunger was designed to compress the moulded pulp into the mould as it would not even be feasible due to this mould only constructing one half of the airframe. Therefore the Nano Plane Mould #1 was placed against a flat surface to force the material flush into the mould; however any attempt at removing excess water would cause the water to be absorbed by the surrounding material. The results from this mould concluded that the moulded fibre would be feasible for pressure moulding.



FIGURE 12 - NANO PLANE MOULD

#### 4.1.2 Beam Mould #1

The second mould that was manufactured; Beam Mould #1 was a complete failure due to the design; however this was assumed a likely outcome. The purpose of this mould was to test the technique of producing two sides of the mould which could each be compacted with moulded pulp before being brought together with some additional moulded pulp to connect the two halves of the casting. The mould was produced from ABS plastic that was 3D printed with hexagonal infill to reduce the amount of material used to reduce costs. An interesting feature that occurred with this 3D print was that the printer was not calibrated correctly which resulted in the final layer being quite sparse; providing a mesh like surface effect. This provided excellent drainage and little improvement was noticed by adding the extra holes for drainage. As this effect was due to a non-calibrated 3D it could not be reproduced on later prints.

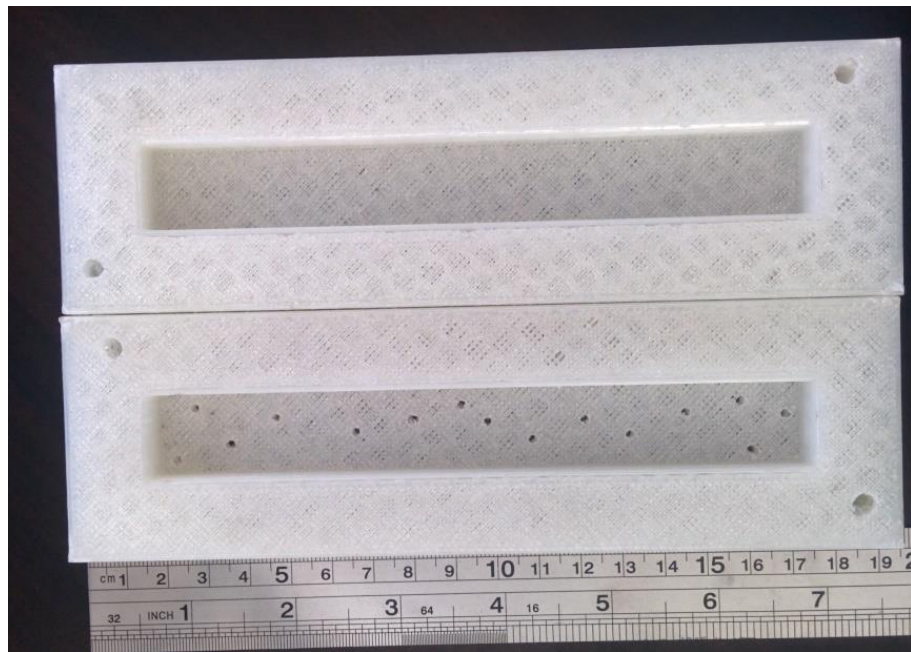


FIGURE 13 - BEAM MOULD #1

#### 4.1.3 Beam Mould #2

Beam Mould #2 was the first compression mould type design which manufactured successful samples seen in Figure 10. The manufactured beams were used in cantilever beam bending experimentation which yielded meaningful data shown in 3.3 Material Testing. The process behind moulding the beams was discussed in 3.2 Beam Manufacturing. The design of the mould was simple due to the shape of the rectangular cross sectioned beam. This became more difficult when moulding airfoils.

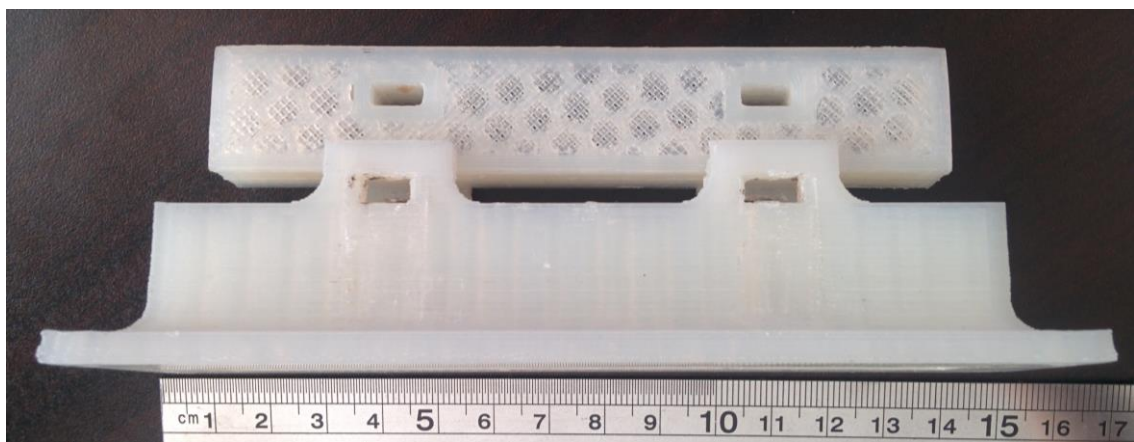


FIGURE 14 - BEAM MOULD #2

Until this point, the design of the proposed airframe was unclear. That is if the design was going to be a flying wing or a traditional aircraft with a tail plane. The results from 3.3 suggested that a flying wing design would be more suited to this material as there would be fewer mould design complexities and locations of stress concentrations involved with the design at connection points. The mould would also require less material to produce, saving in costs.

Based on the success of Beam Mould #2, the following approach was devised to design moulds suitable for airfoils:

1. Find the suitable airfoil for the airframe.
2. Split the airfoil along the mean camber line or chord line into a top and bottom half.
3. From each half, design a surrounding structure that can handle compressive loads. For the bottom half design side walls which act as guides for the top half of the mould so that the leading and trailing edges are aligned. These side walls also ensure that the cardboard slurry is compressed into the mould rather than escaping.
4. Check that the design when assembled produces the desired shape.

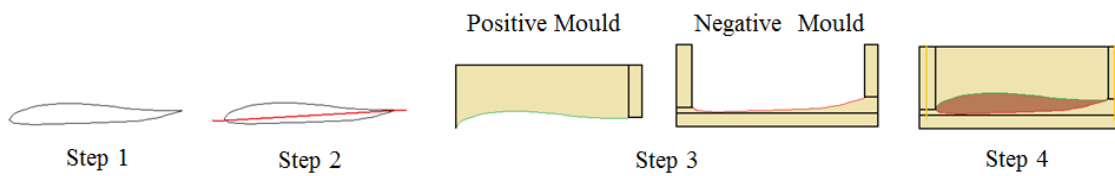


FIGURE 15 - MOULD DESIGN PROCESS FOR AIRFOILS

#### 4.1.4 Limitations Test Mould

The Limitations Test Mould was designed specifically to test possible features that would be required for a dynamically stable flying wing airframe. The features included in this design were:

- Varying airfoils from AG38 root to AG47ct tip
- Varying chord lengths from 150mm root to 100mm tip
- 400mm wing span
- 16° root to tip sweep
- 1.5 taper ratio
- 5° tip twist
- 20° polyhedral

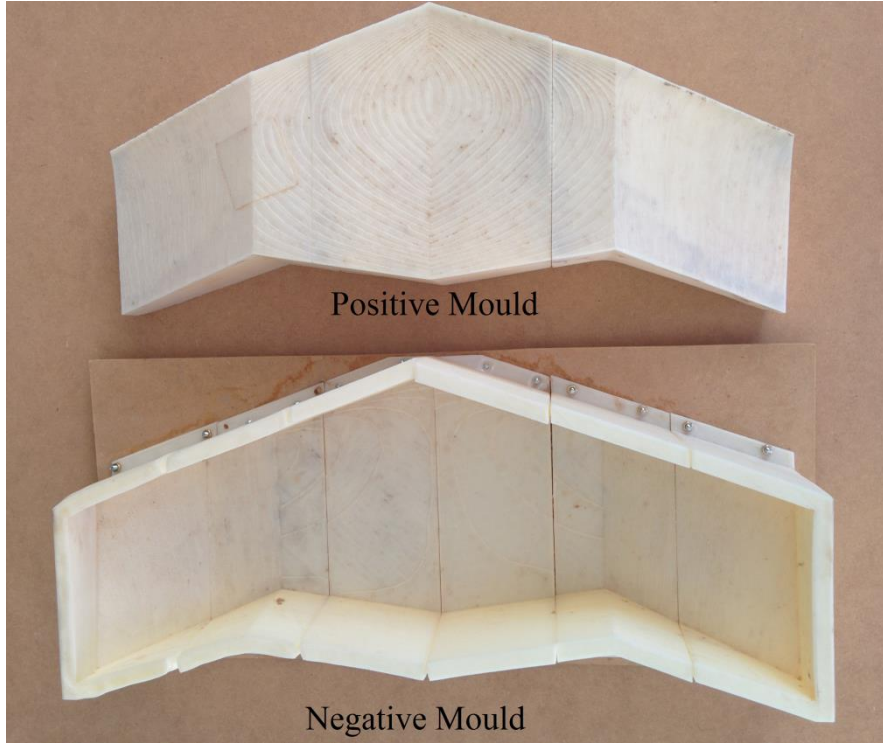


FIGURE 16 - LIMITATIONS TEST MOULD

The design of the mould utilised the process shown in Figure 15. Figure 16 shows the 3D printed Limitations Test Mould which was printed in multiple parts due to the limited print bed size of the FlashForge Creator X ( $225\text{mm} \times 145\text{mm} \times 150\text{mm}$ ) [24]. Therefore each half of the mould needed to be split into sections. From Figure 16 it can be seen that bottom half of the mould consisted of 6 parts whilst the top half of the mould consisted of 3 parts. Through testing it was found that the gaps between mould sections provided adequate drainage.

The airframe size limitation of 400mm was set to satisfy the aim of keeping the airframe simple and cheap to manufacture once the mould was created. This allows for the mould to be placed in a standard 40cm oven resulting in higher throughput of airframe manufacturing.

From the common materials available for 3D printing, ABS was selected over PLA based upon the glass transition temperature of these materials. The glass transition temperature for ABS was  $87.9^\circ\text{C}$  whilst the glass transition temperature for PLA was  $52^\circ\text{C}$ . Therefore ABS would allow for higher curing temperatures over PLA which would result in faster drying. Even though the curing temperature was set to  $75^\circ\text{C}$  for the first production run a section of the mould started to deform. Therefore the curing temperature was reduced to  $65^\circ\text{C}$  and a tolerance of approximately  $20^\circ\text{C}$  was enforced upon any glass transition temperature or maximum service temperature. At this temperature the castings were cured in approximately 6 hours. Ideally a material would be selected

with a glass transition temperature or maximum service temperature well above 100°C so that the excess water would form vapour reducing the overall drying time needed as was found through 3.2 Beam Manufacturing.

Issues common to 3D printing with ABS include warping and shrinkage. It was attempted to reduce the possibility of these issues occurring by enclosing the 3D printer to ensure constant temperature however these issues persisted through. Although the mould surfaces were not affected, it increased the difficulty of inserting the positive mould sections into the negative mould sections as the edges would catch.

The airframes listed in Table 2 were produced using the Limitations Test mould.

TABLE 2 - MANUFACTURED PROTOTYPES FROM LIMITATIONS MOULD

Number	Mass(g)	Max Thickness(mm)
1	59.29	10.62
2	123.68	16.03
3	77.00	12.19
Ideal	81.2	10.5

The first airframe produced was closest to ideal dimensions however the mass; hence density of the moulded fibre was approximately 27% less than the samples calculated from 3.2 Beam Manufacturing. As the mould was slightly deformed during the initial production run, the subsequent products were not ideal as the visual marker to indicate the perfect thickness was destroyed.



FIGURE 17 - SAMPLE 3 FROM LIMITATIONS TEST MOULD

Figure 17 shows the moulded airframe after some basic flash removal. Flash removal could be performed with scissors, razor blades and sand paper. It was imperative that the leading and trailing edges were free from flash and imperfections to ensure that the airfoil could perform as intended.



FIGURE 18 - CLOSEUP OF SURFACE FINISH FROM SAMPLE 3

Due to shrinkage the surface finish on these prototypes were less than ideal as shown in Figure 18, although the replication of the mould lines can also be seen in the finish. The surface finish was increased through sanding, natural gum backed paper tape [25] and beeswax. A combination of beeswax and sanding was found to be the best solution in providing a smoother, waterproof surface which would be necessary for a long range flight. The three sample airframes with various applied smoothing techniques can be seen in Appendix C

#### 4.1.5 Final Mould

The Final Mould was designed around the final airframe which was analysed to be static and dynamically stable in XFLR5 (see 6.3 Stability Design Results and Discussion). The materials explored for the manufacturing of the mould included woods, plastics and metals. The analysis was conducted through a materials selection program called CES which is a powerful materials selection tool.

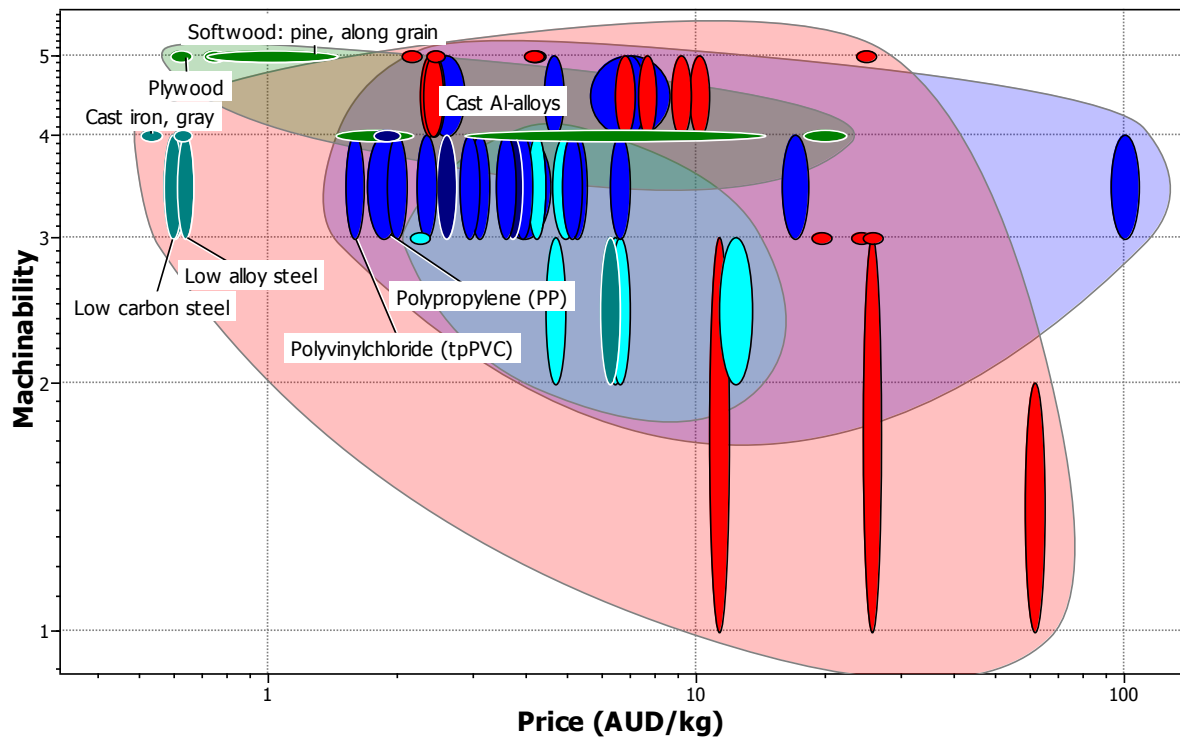


FIGURE 19 – CES 2014 MOULD MATERIAL SELECTION CHART

Figure 15 shows the Machinability vs Price chart which lists Plywood as the most suitable material; however plywood has a maximum service temperature range of 100 – 120 °C which is too low, especially after account for the 20°C tolerance from 4.2.4. Table 2 shows some of the materials in the selection corner; including their maximum service temperature.

TABLE 3 - COMPARISON OF MATERIALS FOR MOULD

Material	Price (AUD/KG)	Machinability	Max Service Temperature
Plywood	0.65	5	100
Pine	1.43	5	120
Cast Iron	0.57	4	450
Low Carbon Steel	0.621	4	400
Low Alloy Steel	0.66	4	550
Polyvinylchloride	1.66	4	70
Polypropylene	2.01	4	115
ABS	3.08	4	76.9
Aluminium	2.53	5	220

For the material to be suitable for the mould it would require a maximum service temperature in excess of 150 degrees. Even though the moulded fibre beams from 3.1.1 were cured at 120°C (not in mould) it would be too precarious to operate at or close to the maximum service temperature of the material. As a natural material wood would need several treatment techniques applied before it

would be possibly suitable for the task; provided that a lower curing temperature was used. Even after these treatments have been applied; the life of the mould would be limited due to the numerous heat cycles with excessive moisture present which could compromise the structural integrity of the mould. This results in only the metals as suitable candidates. Aluminium was chosen as the most suitable as no extra external protective coatings would be required for oxidisation protection.

Based on local supply and availability 4 plates of 420mm × 220mm × 32mm were purchased at an overall cost of \$314.86. Although this exceeded the \$250 budget, the additional funds needed were used from other projects that did not require them. Two plates would be internally bolted together to form each half of the mould after machining. Although the initial cost of the aluminium plate is expensive; it was only a small fraction of the final cost if one considers machining/work time. A total of 20 hours were quoted for the machining time; at a price of \$75 per hour this would equate to \$1500 worth of labour. Thankfully due to the arrangements with the UQ Faculty Workshop Group thesis projects are not charged for work hours; only materials.

One issue that was foreseen with machining the mould was the issue of incorporating drainage due to the method of manufacturing. Using a Computer Numerical Control (CNC) router would leave the finished surface smooth and without gaps for draining. If channels were designed into the machined face; a minimum size of 2mm channels would be used due to tooling limitations. These channels would be large enough for the material to compress and mould into; compromising the design of the airframe. Although it is possible to sand and therefore re-shape cured moulded fibre; this would increase the total manufacturing time of an airframe.

The initial design that was presented and discussed with the UQ Faculty Workshop was similar to that of the Limitations Test Mould. This included side walls designed into the bottom half of the mould to hold excess material before compression; although in a more compact method to save on material costs. The feedback provided resulted in this feature being removed from the base mould as it would significantly increase manufacturing time due to the need for a longer tool bit length; resulting in slower feed rates to avoid destruction of the tool. Therefore it was decided to design the mould as minimalistic as possible; with bolt on side plates on all sides which would fulfil the same role as the previous design. However, just before the contact point for where the leading and trailing edges of the moulds would meet a series of holes were drilled into the side plates for drainage.

Unforeseen delays in regards to the manufacturing of the final mould resulted in the final mould not being produced to exact specification; however the mould appears to function as intended. Based upon these delays the final airframes could not be produced.



FIGURE 20 - FINAL MOULD BOTTOM

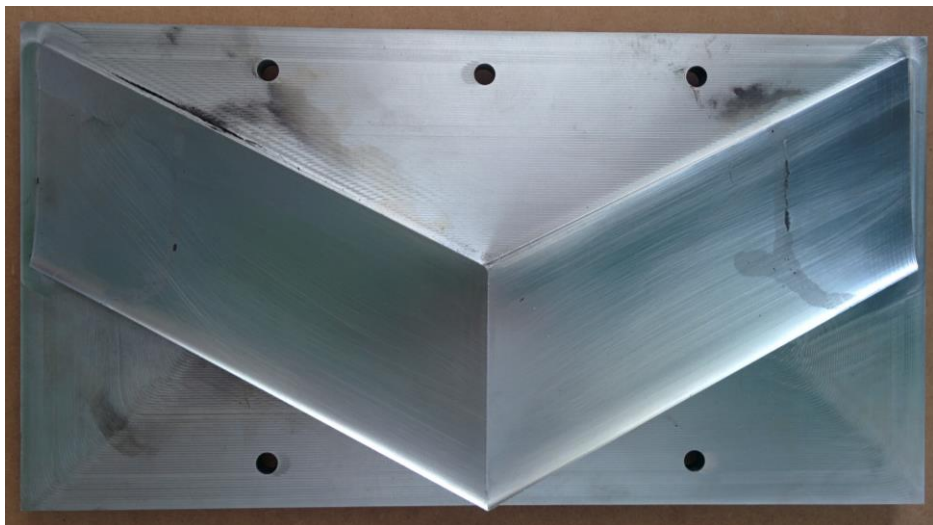


FIGURE 21- FINAL MOULD TOP

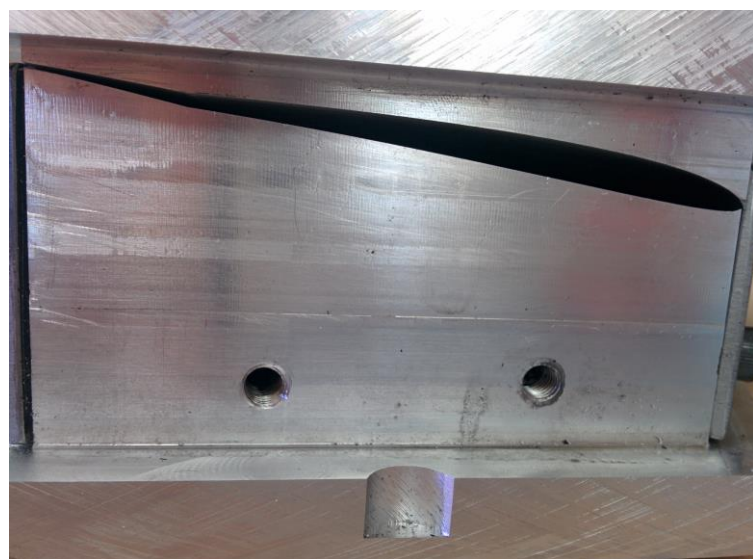


FIGURE 22 - MODIFIED AG19 REFLEX AIRFOIL FROM ASSEMBLED FINAL MOULD

## **5.0 Airfoil Selection**

The airfoil is the primary cause of the aerodynamic forces which in turn act upon the aircraft. Therefore it is paramount that the airfoil selected complies with the design goals for that aircraft in order to complete the intended mission.

### **5.1 Airfoil Selection Methodology**

The primary aim for this glider airfoil is to deliver the maximum glide slope so that the aircraft can travel the maximum distance possible. To ensure that the airfoil delivers the best possible glideslope the airfoil needs to produce a high coefficient of lift and low coefficient of drag. This can be easily compared through polar plots; which compare airfoil properties such as the lift coefficient, drag coefficient, moment coefficient and the angle of attack. Based on the low expected Reynolds numbers (under 100000) the airfoil thickness should not exceed 6% and a camber close to 3% for best performance and glide slope [10] [26]. The aircraft will go through a wide range of Reynolds numbers due to the high altitude launch, therefore polar data must be smooth across wide range of Reynolds numbers to ensure the aircraft behaves in a predictable manner.

Flow separation causing separation bubbles are a common problem at the expected low Reynolds numbers that the airframe is likely to encounter. These separation bubbles have negative effects on aerodynamic performance [27]. To minimize the chance of flow separation occurring the pressure distribution over the airfoil must not have sudden changes in gradient .Therefore the pressure distribution over the airfoil must be analysed to ensure that this does not occur within the intended flight envelope.

As the airframe will be designed based upon a flying wing, it is important that the moment coefficient of the airfoil is close to zero so that the airframe can achieve stability with a combination of sweep, washout, dihedral and additional mass. Reflexed airfoils are commonly used on unswept flying wings due to having a positive moment coefficient although as a trade-off have lower lift to drag ratios [28].

Therefore the airfoil selection is based on the following criteria:

- Lift to drag ratio at  $Re = 50000$ ,  $N_{crit} = 9$ .
- Smooth polar data for wide range of operation
- Maximum thickness of 6%
- Smooth pressure distribution over the airfoil.
- Moment coefficient close to zero to stability can be achieved.

Discuss the requirements for low Re airfoils. Formulas required to estimate Re range (matlab simulation stuff)

## 5.2 Airfoil Simulation and Results

The following airfoils in Table 4 were selected based off the selection criteria and can be seen in Appendix D. It must be noted that many more airfoils were initially compared, the following shown are those that comply with the selection criteria. The Bezier curve airfoils [9] were also tested through XFLR5 however the results were inconclusive due to divergent operational points in the polar plots. The airfoils were also refined locally so that each airfoil was made from 160 panels for equal comparison. The data for  $C_L/C_D$  at  $Re=50000$  was sourced from Airfoil Tools which also provided a basic comparison for the polar data at  $Re = 50000, 100000, 200000, 500000$  and  $1000000$  [29].

TABLE 4 – TABLE OF CANDIDATE AIRFOILS

Airfoil	Max $C_L/C_D$ at $Re=50000$	Alpha at max $C_L/C_D$	Thickness %	Camber %
AG08	32.8	4	5.8	1.7
AG18	35.5	4.25	5.9	2.2
AG19	36.3	4	5.4	2.2
AG47ct	30.5	3.25	5	1.2
Coanda 1	38	4.25	5.7	2.9
GOE 397	42.8	5.75	5.1	4
GOE 587	36.6	4.75	5.8	3
HAM-STD HS1-404	42.1	4.25	4	3.1

These airfoils were also analysed in XFLR5 from a Reynolds number range of 10000 to 70000 with a step size of 10000 to see the operation of the airfoil over the possible expected range of Reynolds numbers. These polar plots can be seen in Appendix E. The pressure distribution of these airfoils was simulated using XFOIL which can be seen in Appendix F.

From the results in Appendix D, Appendix E and Appendix F the airfoil selected for the airframe was the AG19 Mark Drela airfoil [2]. Based on the maximum lift to drag ratios and consistencies of polar plots over the tested Reynolds number range, the AG19 and HAM-STD HS1-404 resulted as the competing airfoils. Although the AG19 airfoil did not satisfy the aim of a 40:1 glideslope, the AG19 had a much smoother pressure distributions along the entire chord, reducing the likelihood of separation bubbles occurring which could potentially result in failure.

## **6.0 Airframe Design**

Although the airframe of the glider will be completely biodegradable the electrical components cannot be. Therefore in the aim of preserving the environmentally friendly nature of the aircraft, the airframe must be designed so that it is inherently stable in both static and dynamic cases. As a result minimal control input would be needed allowing for lower capacity batteries; and less pollutants left in the environment. The chord, span and aspect ratio of the airframe directly affect the estimated gliding range; therefore the effect of these parameters need be analysed.

### **6.1 Airframe Design Methodology**

The primary aim of the airframe was stability; in both static and dynamic cases. Static stability could be easily achieved by balancing out the forces acting upon the aircraft in steady level flight. Dynamic stability was more difficult based upon the oscillatory behaviour from some of these modes which were mentioned in 2.2.8. Therefore the design of the airframe needed to intrinsically dampen the oscillatory effects through the combination of wing sweep, positive dihedral and negative washout. Stability was tested in XFLR5 based upon the results for the wing span and chord length using an iterative technique. Viscous analysis was used due to the extremely low Reynolds numbers.

The airframe must also be designed with the conflicting constraint of gliding distance, ease of manufacturing and material constraints. The constraints of gliding distance and material were tested in MATLAB through a variety of scripts and functions whilst the ease of manufacturing constraint was enforced through a maximum allowable span of 400mm. These scripts and functions would output the estimated distance travelled, time duration, Reynolds number, glideslope and velocity in plots against current altitude based upon the polar data of the AG19 airfoil. These were written with looping in mind so that comparisons between chord length and span could be executed quickly. The MATLAB code that calculated these parameters based upon a given chord and span range was `varyingChordandSpan.m`

Based upon wing loading from chord, span and additional masses (estimated balancing and electronic mass) the structural integrity of the airframe could be assessed. If the calculated mass based upon airfoil area and span length exceeded the calculated allowable mass based on theoretical beam bending for those parameters then the airframe would not be able to support its own weight; causing failure. A safety factor of 2 was enforced to ensure unexpected premature failure would not occur. The MATLAB code that tested the structural integrity of the airframe was `wingBendingLoop.m`

The results listed in 6.2 Airframe Design results were collected using the following method:

1. Generate polar data in XFLR5 for the AG19 airfoil from Reynolds numbers of 5000 to 300000 with a step size of 1000. Export the polar data.
2. Execute the Python script called storeData.py to convert the text file polar data into CSV files.
3. Run varyingChordandSpan.m

Therefore to summarise the airframe design methodology:

- Chord and span were selected based upon the results from MATLAB simulation – taking into account safety factor and aim of the airframe being simple and easy to manufacture.
- Stability would be tested through XFLR5's stability analysis. The airframe would utilise the calculated chord and span, with various amounts of wing sweep, dihedral and washout. Iterative testing would be required until stability in all forms is achieved.

## **6.2 Chord Length and Span Results and Discussion**

The data in Table 5 was gathered by executing the MATLAB script varyingChordandSpan.m showing only the data between the span lengths of 300mm and 400mm. The full range of data from a span of 100mm to 500mm with a chord length varying from 50mm to 150mm can be seen in Appendix G. The simulations initial height was set to 30000m based off realistic weather balloon launch heights [5].

TABLE 5 - RESULTS FROM VARYING CHORD AND SPAN

Span (m)	Chord Length(m)	Max Distance (m)	Mass (kg)	Max Allowable Mass (kg)	Safety Factor
0.3	0.05	444775.7758	0.060056092	0.034735916	0.578391209
0.3	0.06	413974.0622	0.064480773	0.060023663	0.930876908
0.3	0.07	386686.6618	0.069709941	0.095315353	1.367313638
0.3	0.08	362007.8855	0.075743596	0.142278311	1.878420329
0.3	0.09	340442.3444	0.082581739	0.202579861	2.453083007
0.3	0.1	320074.3954	0.090224369	0.277887327	3.079958647
0.3	0.11	300581.2377	0.098671487	0.369868032	3.748479354
0.3	0.12	283262.6558	0.107923092	0.480189301	4.449365671
0.3	0.13	267387.9049	0.117979184	0.610518457	5.174798082
0.3	0.14	252543.7748	0.128839764	0.762522825	5.918381098
0.3	0.15	239266.3768	0.140504831	0.937869728	6.674999852
0.4	0.05	490622.5914	0.063408123	0.026051937	0.410861189
0.4	0.06	466764.7162	0.069307697	0.045017747	0.649534593
0.4	0.07	444535.5637	0.076279921	0.071486515	0.937160311
0.4	0.08	422324.6141	0.084324795	0.106708734	1.265449067
0.4	0.09	402244.7771	0.093442319	0.151934896	1.625975228
0.4	0.1	384945.2855	0.103632493	0.208415495	2.011101826
0.4	0.11	366277.967	0.114895316	0.277401024	2.414380616
0.4	0.12	348225.9841	0.127230789	0.360141976	2.830619674
0.4	0.13	331018.8593	0.140638913	0.457888843	3.255776332
0.4	0.14	315529.8005	0.155119686	0.571892119	3.686779771
0.4	0.15	300355.6413	0.170673108	0.703402296	4.12134227

From the data shown in Table 5 and Appendix G it was apparent that there was a direct correlation between wing span, chord length and maximum distance travelled. This was due to the direct relationships between the Reynolds number, lift, velocity, sink rate, aspect ratio and induced drag. As the chord length increased, the Reynolds number, mass and lift would also increase whilst the aspect ratio would decrease. Increases in Reynolds number would increase the coefficients of lift and drag, therefore altering velocity, glideslope and sink rate. However due to the decrease in aspect ratio, the induced drag would increase – lowering the glideslope and increasing sink rate.

From these results a span of 400mm and chord length of 100mm were selected due to the achieving the furthest distance travelled whilst satisfying the criteria of a safety factor greater than 2. The 400mm span would also allow for the mould to fit within a standard 600mm oven with minimum internal dimensions of 420mm. Although the distance travelled was approximate half of the intended 750km for the ideal flight from Sydney to Brisbane; it would not be possible with moulded fibre due to the mechanical limitations of the material. A high aspect ratio wing would be required to reduce induced drag and trailing vortices as discussed in section 2.2.3. A solution found to achieve the 750km distance was an airframe that had a wing span of 1800mm with a chord length of

200mm. However, due to the excessive mass of the wing the resultant safety factor was 0.365; meaning that the wing would not be able to support its own weight.

To assist in the understanding of the aerodynamic variables a MATLAB script called planeSim.m was created. For each decremented step in altitude the aerodynamic variables were stored with reference to the altitude. Provided with a chord of 100mm and a span of 400mm the Figure 24 were created showing how the change in altitude varied the distance travelled, Reynolds number and velocity. A full set of figures for each aerodynamic variable can be seen in Appendix H. The Reynolds number range was 10883 to 53087.

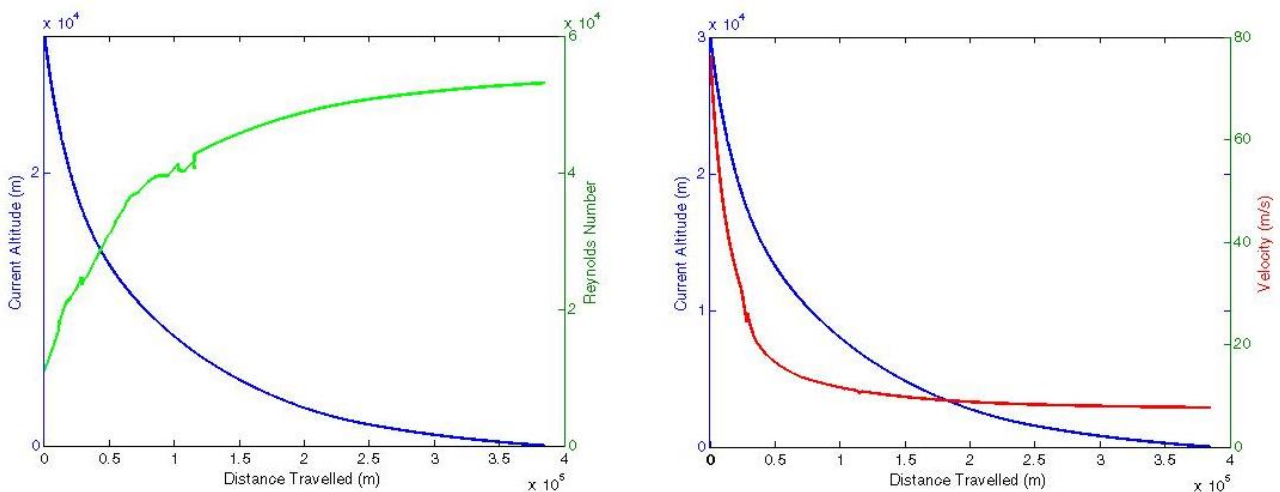


FIGURE 23 - PLANESIM.M PLOTS

Figure 23 shows that the aircraft rapidly loses altitude due to extremely low Reynolds numbers for the first 100000m travelled. Once the aircraft reaches Reynolds numbers of approximately 40000 the aerodynamic variables reach sufficient values so that the airframe can perform as intended.

### 6.3 Stability Design Results and Discussion

To achieve stability in all 8 stability modes, the airframe was designed with the following:

- Wing span of 400mm
- Chord length of 100mm
- AG19 root airfoil
- AG19 -6° reflex tip airfoil with -6° tip twist
- 26° wing sweep
- 10° positive dihedral
- 50g balancing mass placed 2cm from the leading edge
- 110g total mass

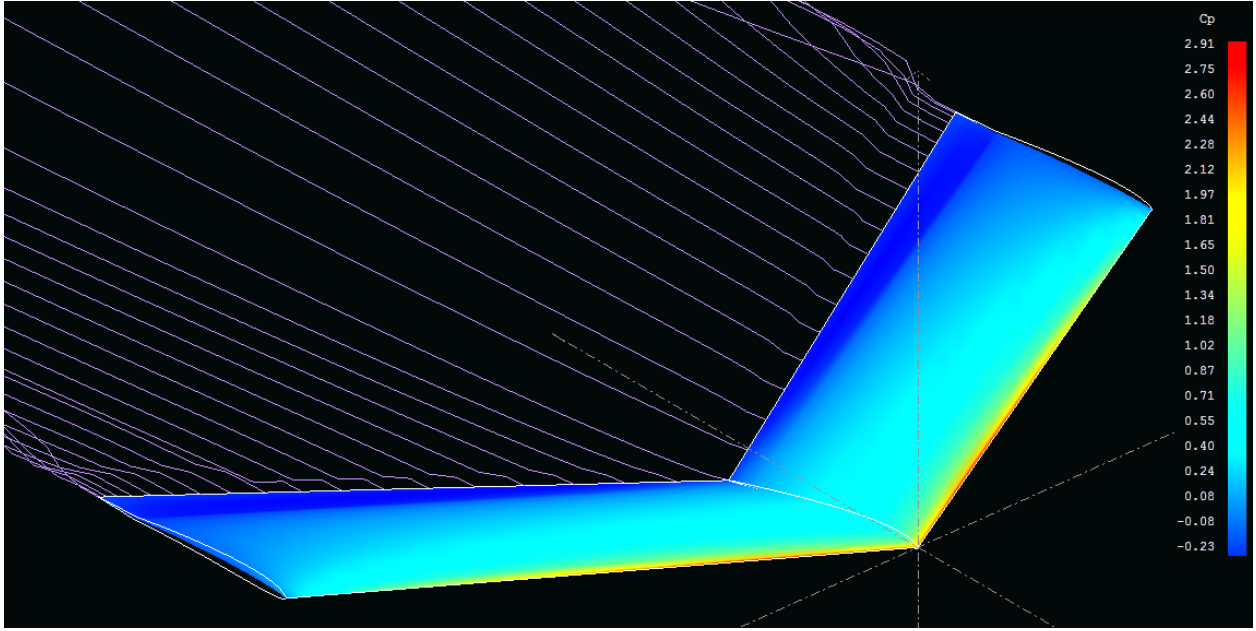


FIGURE 24 - FINAL AIRFRAME DESIGN IN XFLR5

These stability enhancing features reduced the overall glideslope from 13 at an angle of attack of  $4^\circ$  based upon an ideal flying wing of the same airfoil and dimensions to 11.2 at an angle of attack of  $10^\circ$ . The slight reduction in glideslope was considered an appropriate trade-off for a stable airframe.

A guide for XFLR5 stability analysis was followed to produce the final stable design [30]. The damping plots based on the XFLR5 results can be seen in Appendix I. The polar plots for some of the designs tested can be seen in Appendix J. These designs included variations of the final design with tapered wings and wing plates however these were found to negatively affect the glide slope of the airframe. This was possibly due to low Reynolds numbers and the viscous flow analysis used as initial tests of wing plates with inviscid flow and higher Reynolds numbers resulted in increased airframe efficiency. These initial tests using inviscid flow are attached in Appendix K.

Designs for stable airframes were initially tested based upon parameters found through design guides [31] [32]. The issues with the design guides are that the formulas provided did not work on small spans and chord lengths. An example of this was the Pankin twist formula suggesting a  $-31.8^\circ$  twist at the wing tips to provide stability based upon the parameters listed above. Using a tip twist of  $-31.8^\circ$  would result in extreme amounts of drag and moment that would not result in a useful airframe. Therefore iterative testing through XFLR5 was found to be the best solution as a MATLAB based simulator for stability could not be created in time.

The Dutch roll modes were the hardest to satisfy. This was due to the yaw component of the stability mode as the airframe designed did not have a tailplane. This was overcome through the use

of the modified AG19 airfoil with -6° reflex at the tip of the wing in combination with the -6° tip twist or washout.

The additional 50g balancing mass was required 2cm from the leading edge of the root chord to shift the centre of gravity further away from the neutral point. This was in order to achieve static and therefore dynamic stability. This mass could be comprised of the electrical components and ballast. To decrease the possible drag that the electrical components could induce on the airframe, it would be suggested to design a bulbous nose from beeswax that could contain the electrical components. This would shield the electrical components from the elements and decrease the negative aerodynamics caused by the shape of these components.

## 7.0 Conclusion

This thesis was separated into 4 individual parts, these were:

1. Understanding Moulded Pulp
2. Mould Design
3. Airfoil Selection
4. Airframe Design

From the Understanding Moulded Pulp section the mechanical properties were tested through cantilever beam bending experimentation. The results found from this were deemed accurate through correlation with the thesis paper *Packaging Systems Redesign: A Study in Designing More Sustainable Product Packaging Systems* [1].

Understanding the mechanical and physical properties of moulded pulp allowed for moulds to be designed which could produce airfoils. The techniques used in industry would not have been able to produce airfoils; hence a compression moulding method was used. Utilising a compression moulding technique satisfied the project aim of keeping the manufacturing process simple in comparison to the industry techniques. The produced airframes required finishing in the form of sanding and waterproofing to ensure that the airfoil was smooth and would perform as simulated.

The airfoil selected was the AG19 Mark Drela airfoil [2]. This selection was based upon the criteria that the airfoil needed to be below a 6% thickness, provide a high lift to drag ratio and have a smooth pressure distribution curve in order to prevent flow separation. Although the lift to drag ratio of the AG19 airfoil fell short just short of the 40:1 glideslope at a Reynolds number of 50000, the trade-off for smoother pressure distribution was made.

The chord and span lengths of the airframe were evaluated through MATLAB scripts which resulted in a 400mm wing span and a 100mm chord length. Although this would not provide the ideal flight from Sydney to Brisbane, a flight of approximately 384945m could be achieved based upon the Reynolds number range from 10883 to 53087. Through this simulation it was found that a wing span of 1800mm and a chord length of 200mm would be needed to attain this distance however the wing loading would be too great for the structural integrity of the wing to be held.

A stable airframe was designed in XFLR5 with a combination of stability enhancing features for a slight reduction in overall glideslope. This was considered an appropriate compromise to ensure that the airframe could maintain a constant flight path based on minimal control input. This would allow for lower capacity batteries which would reduce the impact to the environment after mission completion.

This work can be continued by testing the final mould that was designed and manufactured. Ideally this would have been tested within this project; however unforeseen delays in the mould manufacturing stopped this from happening. The work can be improved by searching for natural ways of improving the stiffness of moulded fibre to allow for higher aspect ratio wings and therefore longer flight distances. Another thesis project could be undertaken to design an extremely low power control system to guide the airframe to the intended target. Research into biodegradable electronic components could also be suggested to coincide with the environmentally friendly nature of the disposable and biodegradable UAV.

## Appendix A

Appendix A contains the results for research from the Nanjing University of Technology for the compression resistance and cushioning properties of the various moulded fibre materials tested [13].

**Table-1. Properties of fruit trays prepared from different pulp fiber sources.**

Sample Name	Fiber source	Average quantity (g)	Average thickness (mm)
A	Bamboo pulp	68.5	0.865
B	Bamboo & TMP (30%wt)	76.55	0.877
C	Bamboo & TMP (40%wt)	69.36	0.753
D	Newspaper pulp	66.5	0.85
E	Newspaper & TMP(40%wt)	68.5	0.803
F	Corrugated box pulp	81.8	0.83

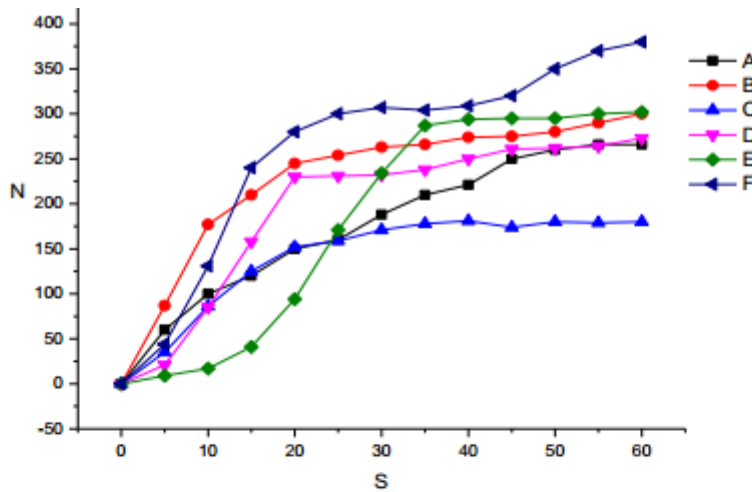


**Figure 5. The resistance of compression properties of 6 types of fruit trays (Left). (A, B, C, D, E, F as shown in Table-1 above).**

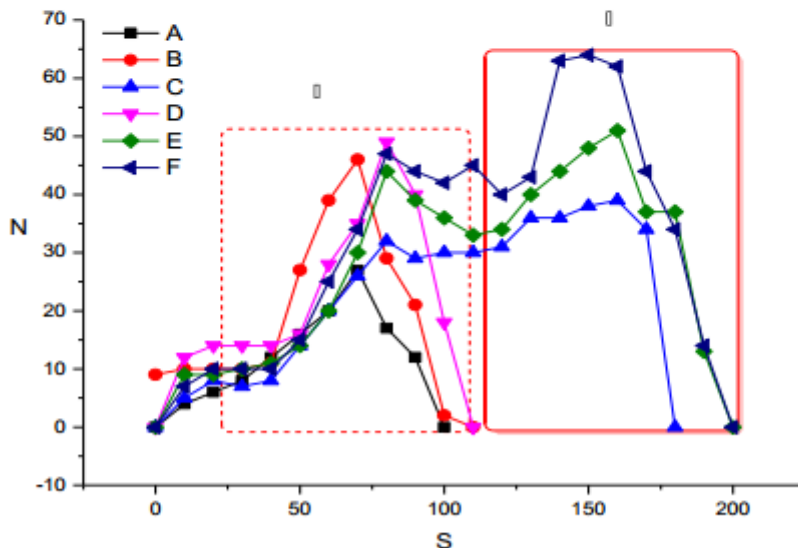


**Figure 6. The cushioning properties of cushion structure in six types of fruit trays (Right). (A, B, C, D, E, F as shown in Table-1 above).**

## Appendix B

Appendix B contains the data gathered and results found from the equations listed in Beam Bending Theory

Beam1	Mass(gram)	9.9	Dimensions(LxWxH)(mm)	0.1149	0.0139	0.0141	1	3.24706E-09										Wet Dimensions	0.1172	0.0144	0.0151	
Mass(grams)	0	100	200	300	400	500	600	700	800	900	1000	Area_c	0.00019599	L0	0.0849		Volume	2.2519E-05 m <sup>3</sup>				
Y Displacement(mm)	6.5	7	7.5	8	9	9.5	10.5	12	14 break			Area Mom	3.24706E-09 m <sup>4</sup>	L	0.085231		Density	439.623858 kg/m <sup>3</sup>				
Normalized	0	0.5	1	1.5	2.5	3	4	5.5	7.5 break			Moment	0.62784 Nm				Shrinkage	4.01906537 %				
												Y	0.00705 m									
												Stress_x	1363161.169 Pa	Strain_x	0.003894	Young's Modulus	350.037743 Mpa					
Beam2	Mass(gram)	10.5	Dimensions(LxWxH)(mm)	0.1145	0.0138	0.0142						Area_c	0.00019596	L0	0.0845		Wet Dimensions	0.1173	0.0146	0.0155		
Mass(grams)	0	100	200	300	400	500	600	700	800	900	1000	Area Mom	3.29278E-09 m <sup>4</sup>	L	0.084926		Volume	2.2437E-05 m <sup>3</sup>				
Y Displacement(mm)	2.5	3	3.5	4.5	5	6	7.5	9	11 break			Moment	0.62784 Nm				Density	467.968242 kg/m <sup>3</sup>				
Normalized	0	0.5	1	2	2.5	3.5	5	6.5	8.5 break			Y	0.0071 m				Shrinkage	5.41786353 %				
												Stress_x	1353768.662 Pa	Strain_x	0.005047	Young's Modulus	268.252944 Mpa					
Beam3	Mass(gram)	10.6	Dimensions(LxWxH)(mm)	0.115	0.0138	0.015						Area_c	0.000207	L0	0.085		Wet Dimensions	0.1173	0.0148	0.016		
Mass(grams)	0	100	200	300	400	500	600	700	800	900	1000	Area Mom	3.88125E-09 m <sup>4</sup>	L	0.085288		Volume	2.3805E-05 m <sup>3</sup>				
Y Displacement(mm)	2.5	3	3.5	4	4.5	5.5	6.5	8	9.5 break			Moment	0.62784 Nm				Density	445.284604 kg/m <sup>3</sup>				
Normalized	0	0.5	1	1.5	2	3	4	5.5	7 break			Y	0.0075 m				Shrinkage	4.98918036 %				
												Stress_x	1213217.391 Pa	Strain_x	0.003385	Young's Modulus	358.380916 Mpa					
Beam4	Mass(gram)	6.4	Dimensions(LxWxH)(mm)	0.1145	0.0139	0.0102						Area_c	0.00014178	L0	0.0845		Wet Dimensions	0.1172	0.0147	0.0114		
Mass(grams)	0	100	200	300	400	500	600	700	800	900	1000	Area Mom	1.22923E-09 m <sup>4</sup>	L	0.084537		Volume	1.6234E-05 m <sup>3</sup>				
Y Displacement(mm)	2.5	3.5	5 break									Moment	0.15696 Nm				Density	394.238937 kg/m <sup>3</sup>				
Normalized	0	1	2.5 break									Y	0.0051 m				Shrinkage	6.09074898 %				
												Stress_x	651216.0514 Pa	Strain_x	0.000438	Young's Modulus	1488.27607 Mpa					
Beam5	Mass(gram)	6.8	Dimensions(LxWxH)(mm)	0.1144	0.0138	0.0103						Area_c	0.00014214	L0	0.0844		Wet Dimensions	0.117	0.0145	0.0115		
Mass(grams)	0	100	200	300	400	500	600	700	800	900	1000	Area Mom	1.25664E-09 m <sup>4</sup>	L	0.084495		Volume	1.6261E-05 m <sup>3</sup>				
Y Displacement(mm)	4	5	6	8 break								Moment	0.23544 Nm				Density	418.183196 kg/m <sup>3</sup>				
Normalized	0	1	2	4 break								Y	0.00515 m				Shrinkage	5.82819701 %				
												Stress_x	964890.3515 Pa	Strain_x	0.001122	Young's Modulus	859.639841 Mpa					
Beam6	Mass(gram)	7.3	Dimensions(LxWxH)(mm)	0.1138	0.0138	0.0115						Area_c	0.0001587	L0	0.0838		Wet Dimensions	0.1173	0.015	0.0137		
Mass(grams)	0	100	200	300	400	500	600	700	800	900	1000	Area Mom	1.74901E-09 m <sup>4</sup>	L	0.08398		Volume	1.806E-05 m <sup>3</sup>				
Y Displacement(mm)	1.5	2.5	3.5	4.5	7 break							Moment	0.31392 Nm				Density	404.206852 kg/m <sup>3</sup>				
Normalized	0	1	2	3	5.5 break							Y	0.00575 m				Shrinkage	9.01406546 %				
												Stress_x	1032037.478 Pa	Strain_x	0.002151	Young's Modulus	479.683813 Mpa					
Beam7	Mass(gram)	8.5	Dimensions(LxWxH)(mm)	0.1133	0.0141	0.0141						Area_c	0.00019881	L0	0.0833		Wet Dimensions					
Mass(grams)	0	100	200	300	400	500	600	700	800	900	1000	Area Mom	3.29378E-09 m <sup>4</sup>	L	0.083637		Density		377.355592 kg/m <sup>3</sup>			
Y Displacement(mm)	2.5	3.5	4	4.5	5	6	7	8	10 break			Moment	0.62784 Nm									
Normalized	0	1	1.5	2	2.5	3.5	4.5	5.5	7.5 break			Y	0.00705 m									
												Stress_x	1343825.549 Pa	Strain_x	0.004045	Young's Modulus	332.21394 Mpa					
Beam8	Mass(gram)	8.9	Dimensions(LxWxH)(mm)	0.1152	0.0141	0.0138						Area_c	0.00019458	L0	0.0852		Wet Dimensions					
Mass(grams)	0	100	200	300	400	500	600	700	800	900	1000	Area Mom	3.08798E-09 m <sup>4</sup>	L	0.085728		Density		397.044632 kg/m <sup>3</sup>			
Y Displacement(mm)	6	6.5	7	7.5	8	9	10	11	12.5	15.5 break		Moment	0.70632 Nm									
Normalized	0	0.5	1	1.5	2	3	4	5	6.5	9.5 break		Y	0.0069 m									
												Stress_x	1578248.803 Pa	Strain_x	0.006197	Young's Modulus	254.671921 Mpa					
Beam9	Mass(gram)	8.2	Dimensions(LxWxH)(mm)	0.1134	0.0138	0.0138						Area_c	0.00019044	L0	0.0834		Wet Dimensions					
Mass(grams)	0	100	200	300	400	500	600	700	800	900	1000	Area Mom	3.02238E-09 m <sup>4</sup>	L	0.083653		Density		379.701773 kg/m <sup>3</sup>			
Y Displacement(mm)	3.5	4	4.5	5	5.5	6.5	7.5	8.5	10 break			Moment	0.62784 Nm									
Normalized	0	0.5	1	1.5	2	3	4	5	6.5 break			Y	0.0069 m									
												Stress_x	1433385.387 Pa	Strain_x	0.003033	Young's Modulus	472.668179 Mpa					
Beam10	Mass(gram)	2.7	Dimensions(LxWxH)(mm)	0.117	0.0144	0.0135						Area_c	0.0001944	L0	0.087							
Mass(grams)	0	100	200	300	400	500	600	700	800	900	1000	Area Mom	2.95245E-09 m <sup>4</sup>	L	0.087323		Density		118.708452 kg/m <sup>3</sup>			
Y Displacement(mm)	7	8.5	10	12	14.5	35	49	60	71	78 beyond useable		Moment	0.31392 Nm									
Normalized	0	1.5	3	5	7.5	28	42	53	64	71		Y	0.00675 m									
												Stress_x	717695.4733 Pa	Strain_x	0.003709	Young's Modulus	193.504389 Mpa					

Use 80mm for moment arm for stress results (Approx 20mm in vice, 15mm from edge to where mass was applied)

Avg Max Stress  
Mpa

Avg Density 413.7342 kg/m<sup>3</sup>

Avg Shrinkage 5.893187

Lowest Max Stress 1.213217 MPa

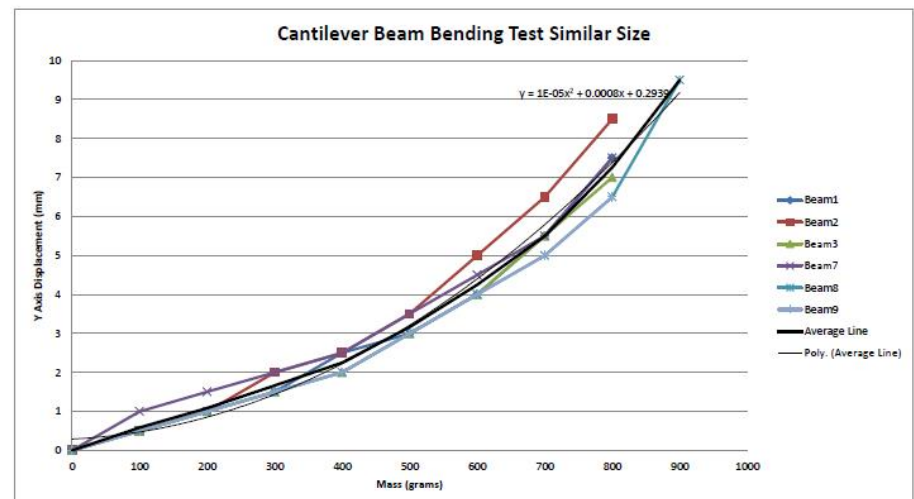
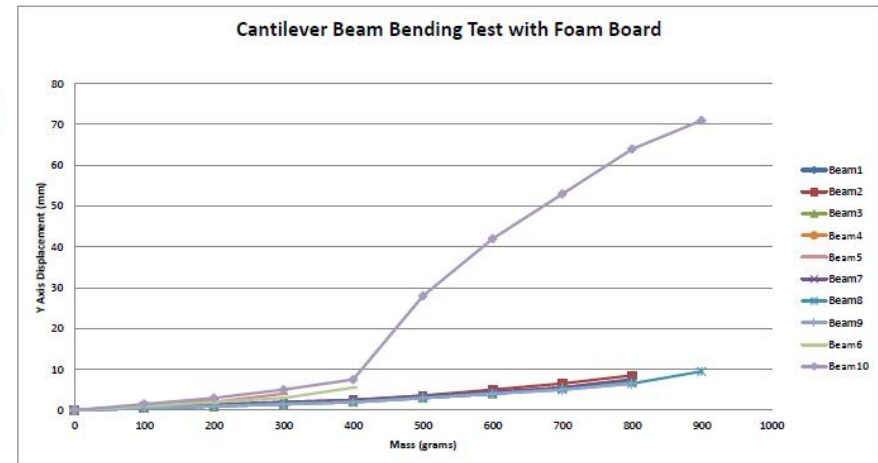
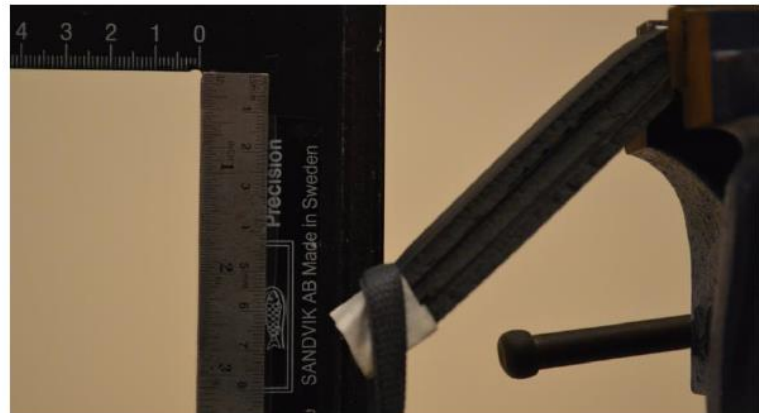
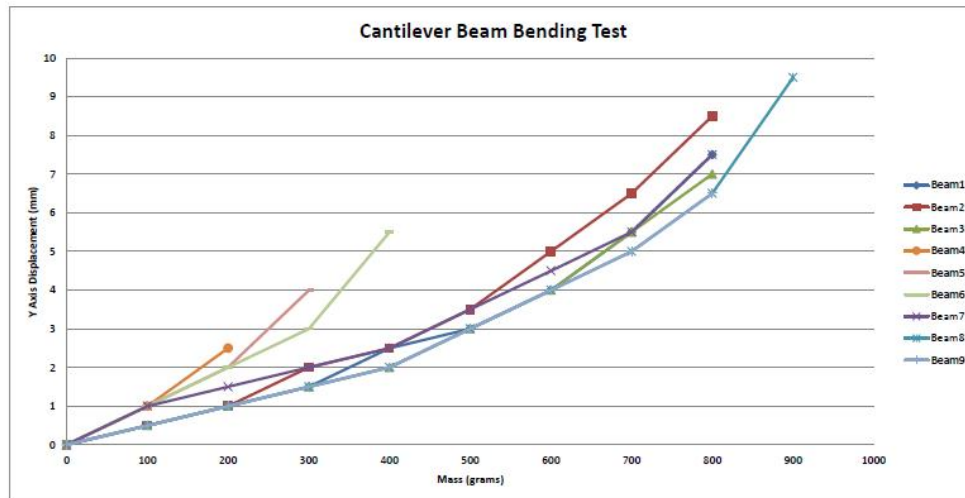
Lowest Max Strain 0.003033

Lowest E 254.6719

Avg E 339.3709

Wet Dimensions

Beam1	0	0.5	1	1.5	2.5	3	4	5.5	7.5
Beam2	0	0.5	1	2	2.5	3.5	5	6.5	8.5
Beam3	0	0.5	1	1.5	2	3	4	5.5	7
Beam7	0	1	1.5	2	2.5	3.5	4.5	5.5	7.5
Beam8	0	0.5	1	1.5	2	3	4	5	6.5
Beam9	0	0.5	1	1.5	2	3	4	5	6.5
	0	0.583333	1.083333	1.666667	2.25	3.16666667	4.25	5.5	7.25



## Appendix C

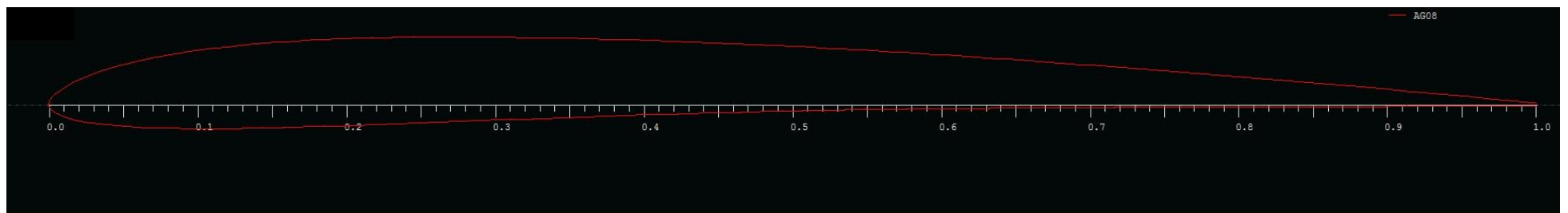
Appendix C contains the 3 prototypes created with the Limitations Test Mould. Sample 1 was coated with Beeswax for a waterproof coating. Attempts at increasing surface finish with thick layers of Beeswax seemed to work however added large amount of additional mass. Sample 2 was wrapped partially in natural gummed tape. This significantly increased the surface finish however was not waterproof. Sample 3 is essentially straight out of the mould, other than flash removal.



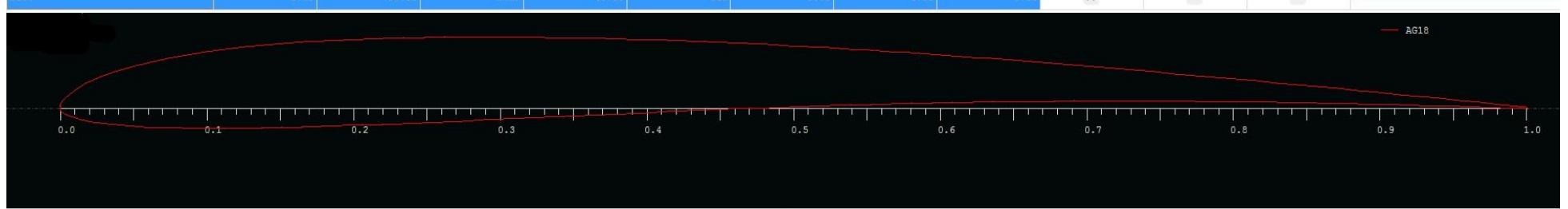
## Appendix D

Appendix D contains the airfoils listed in Table 4 as seen through XFLR5. Note: 160 points were used for airfoil when computing the polar data.

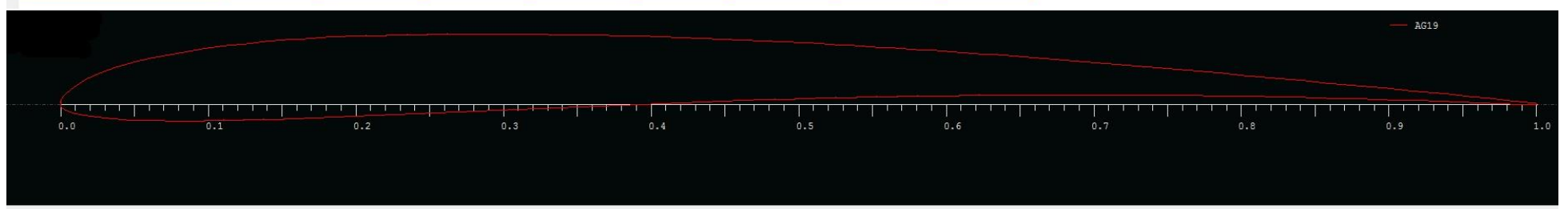




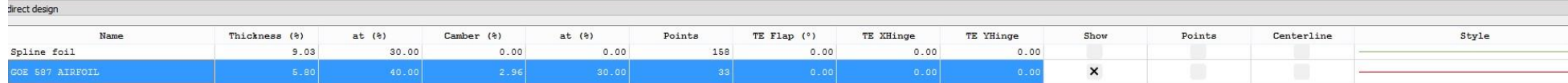
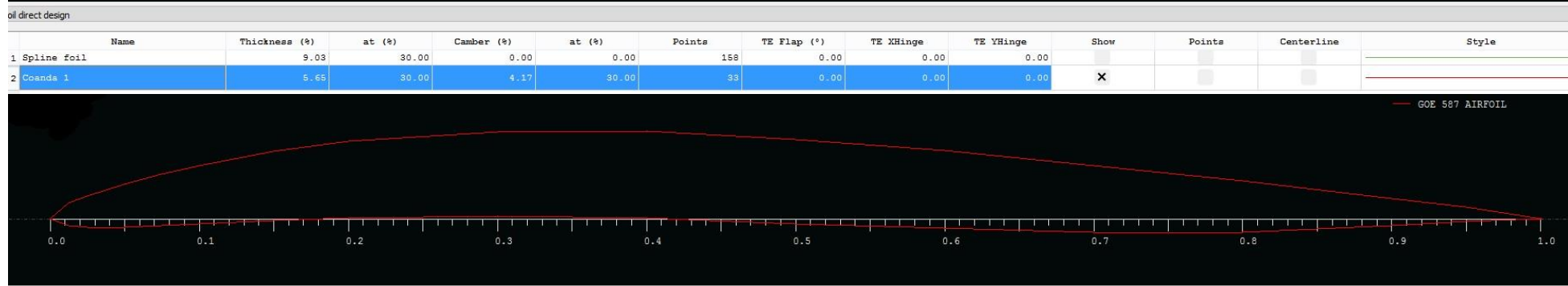
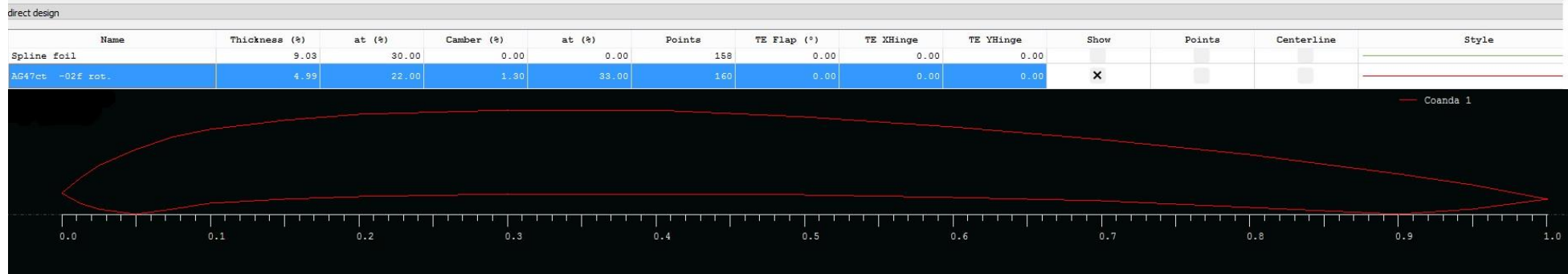
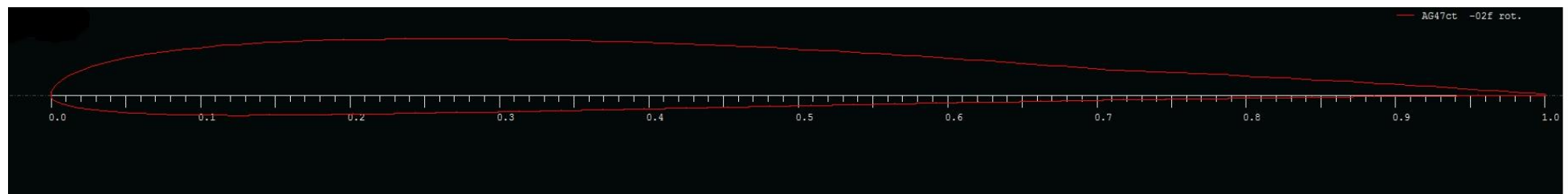
direct design												
Name	Thickness (%)	at (%)	Camber (%)	at (%)	Points	TE Flap (°)	TE XHinge	TE YHinge	Show	Points	Centerline	Style
Spline foil	9.03	30.00	0.00	0.00	158	0.00	0.00	0.00				
AG08	5.83	21.00	1.80	40.00	160	0.00	0.00	0.00	X			

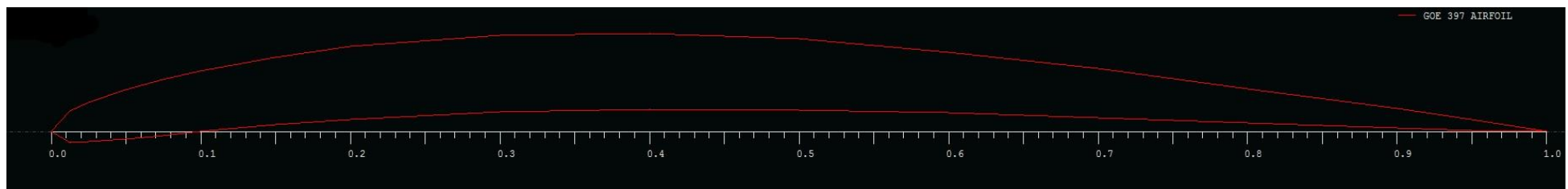


oil direct design												
Name	Thickness (%)	at (%)	Camber (%)	at (%)	Points	TE Flap (°)	TE XHinge	TE YHinge	Show	Points	Centerline	Style
1 Spline foil	9.03	30.00	0.00	0.00	158	0.00	0.00	0.00				
2 AG18	5.87	21.00	2.16	44.00	160	0.00	0.00	0.00	X			

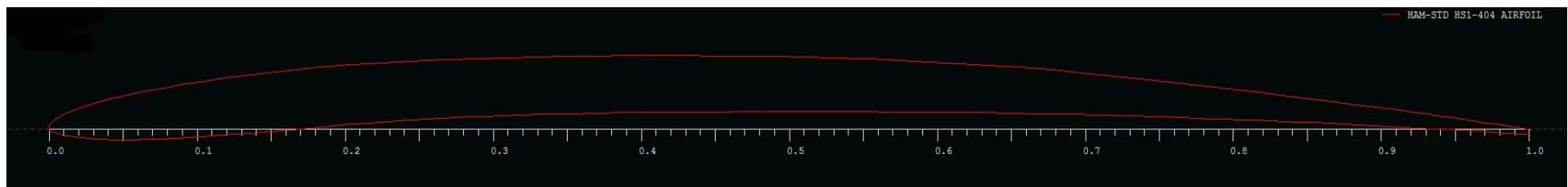


oil direct design												
Name	Thickness (%)	at (%)	Camber (%)	at (%)	Points	TE Flap (°)	TE XHinge	TE YHinge	Show	Points	Centerline	Style
1 Spline foil	9.03	30.00	0.00	0.00	158	0.00	0.00	0.00				
2 AG19	5.40	20.00	2.27	43.00	160	0.00	0.00	0.00	X			





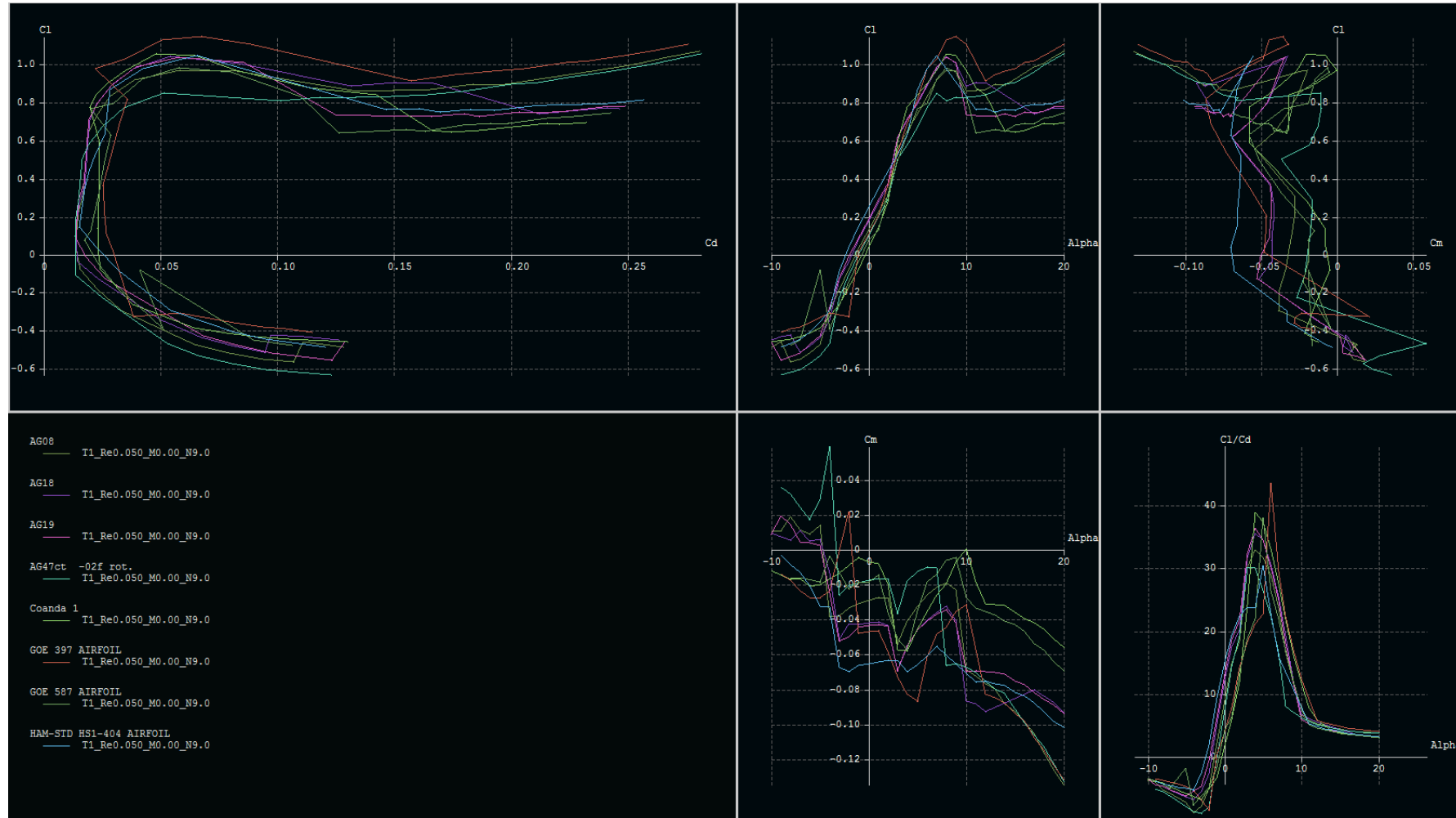
direct design												
Name	Thickness (%)	at (%)	Camber (%)	at (%)	Points	TE Flap (°)	TE XHinge	TE YHinge	Show	Points	Centerline	Style
Spline foil	9.03	30.00	0.00	0.00	158	0.00	0.00	0.00				
GOE 397 AIRFOIL	5.10	30.00	3.96	40.00	33	0.00	0.00	0.00	X			

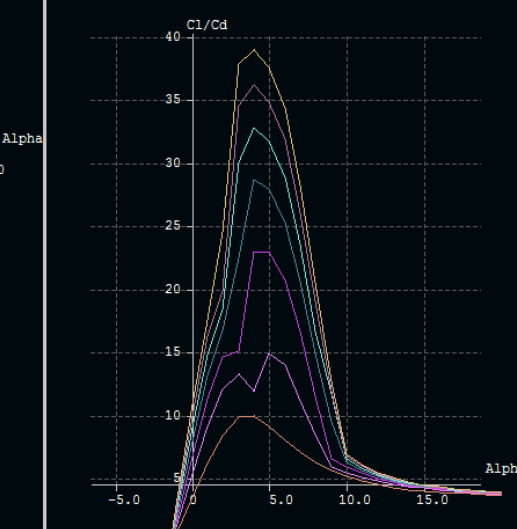
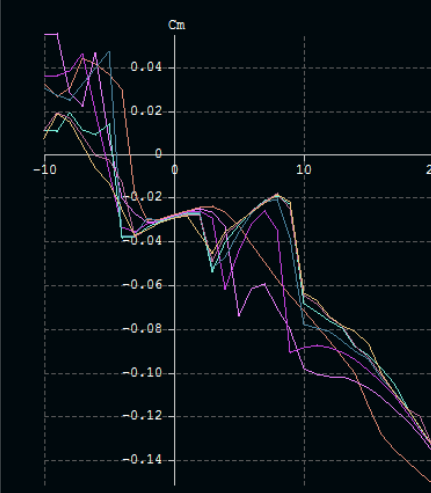
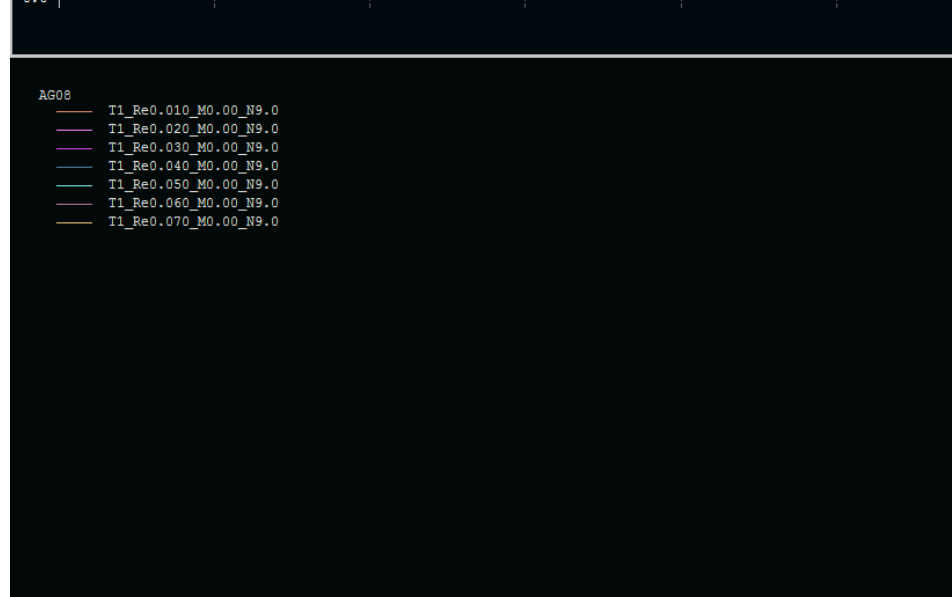
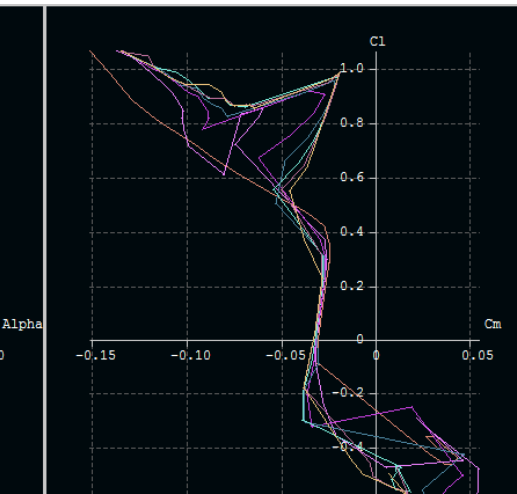
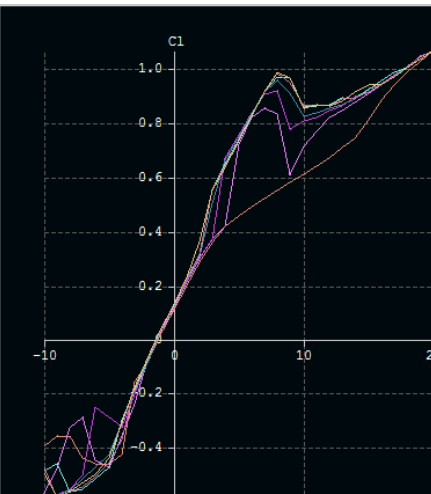
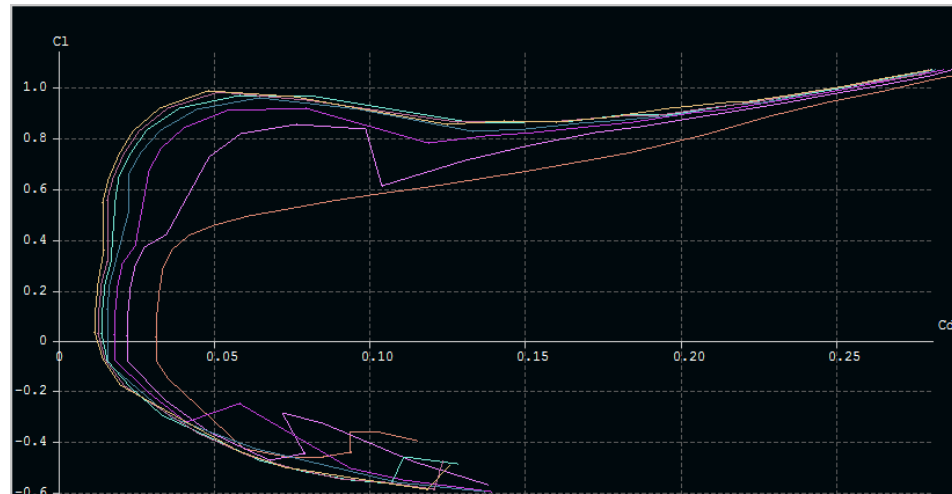


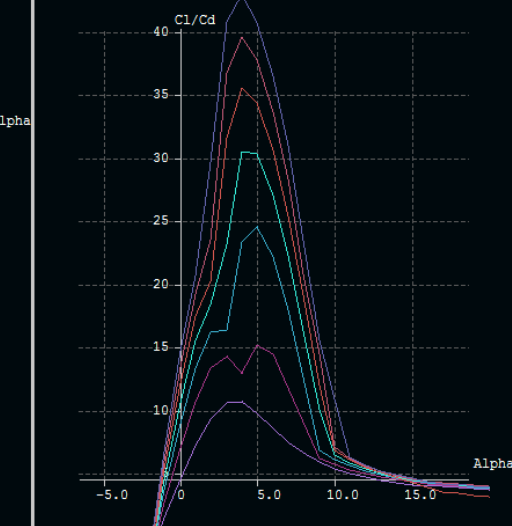
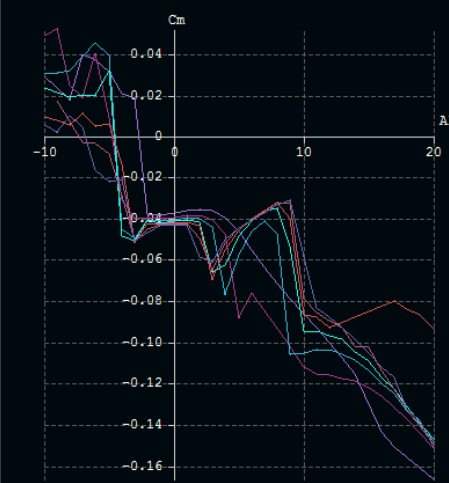
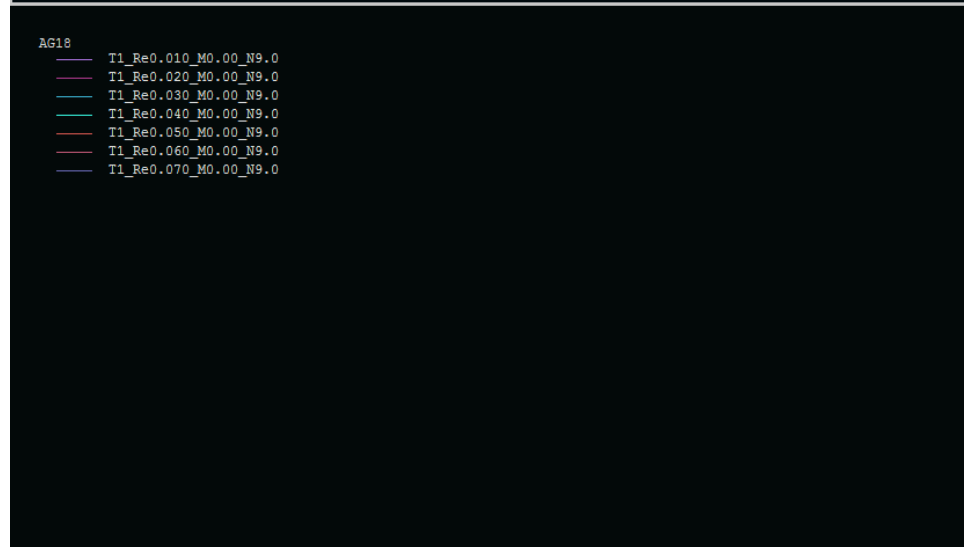
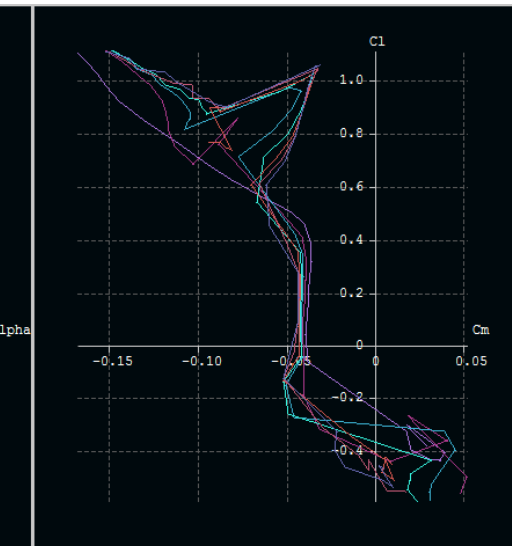
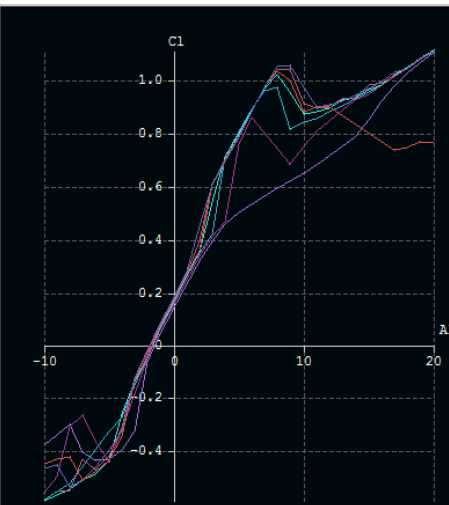
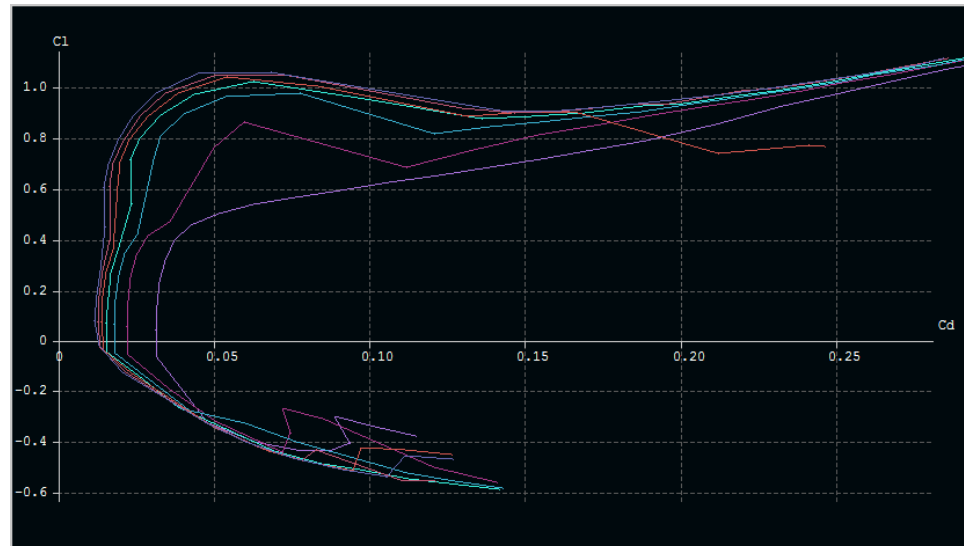
direct design												
Name	Thickness (%)	at (%)	Camber (%)	at (%)	Points	TE Flap (°)	TE XHinge	TE YHinge	Show	Points	Centerline	Style
Spline foil	9.03	30.00	0.00	0.00	158	0.00	0.00	0.00				
HAM-STD HS1-404 AIRFOIL	4.02	18.00	3.01	44.00	124	0.00	0.00	0.00	X			

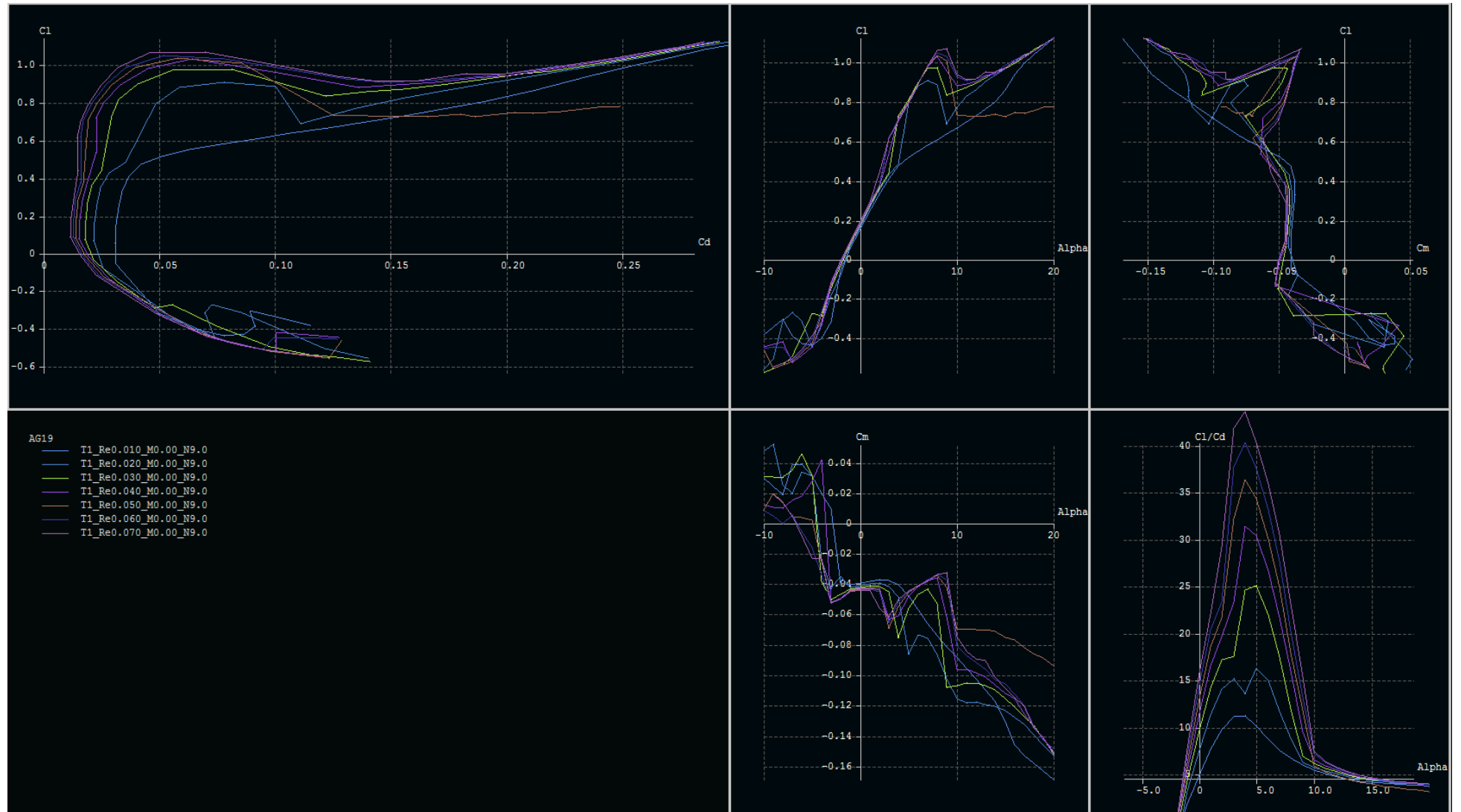
## Appendix E

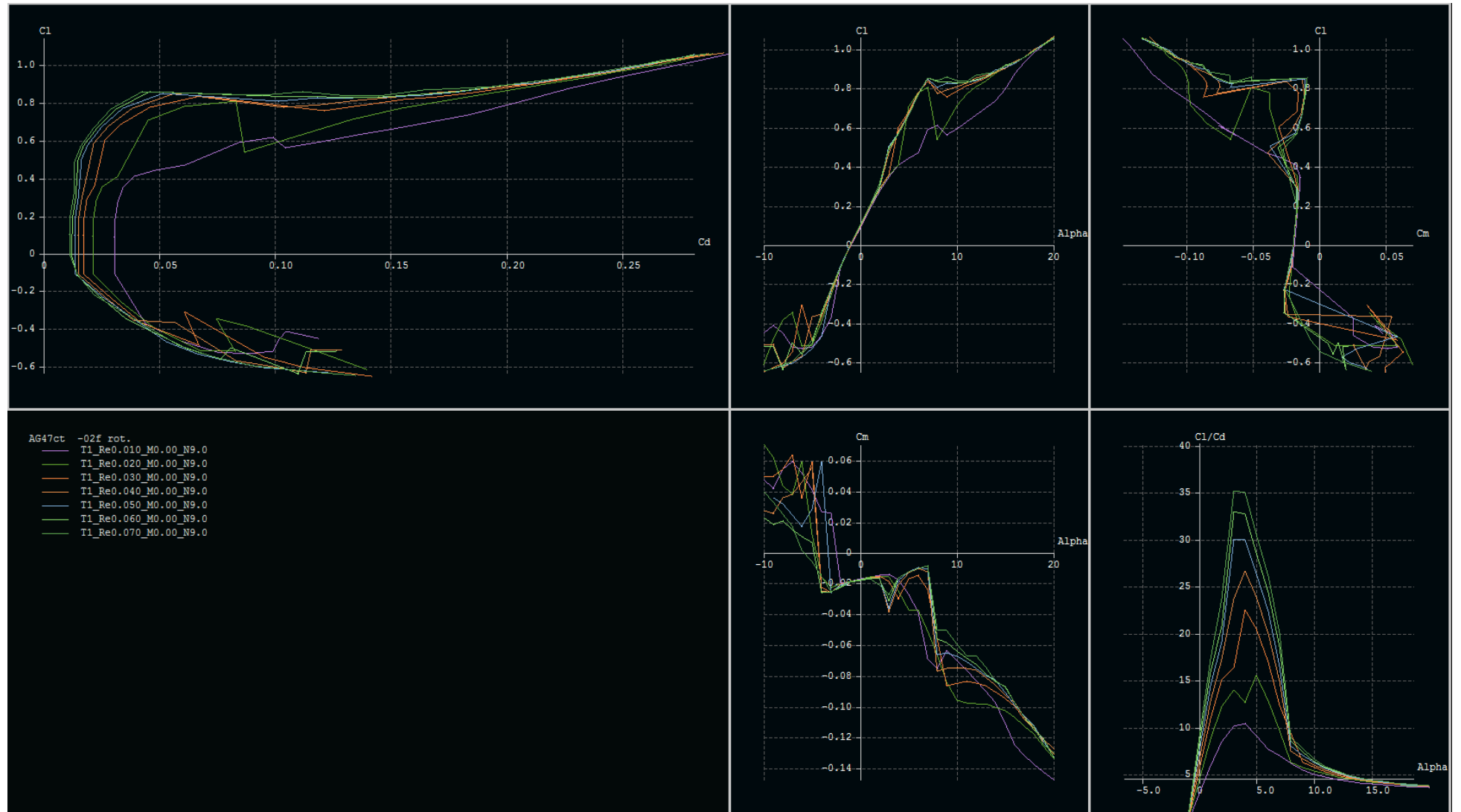
Appendix E contains the polar plots for the airfoils listed in Appendix D. These were computed in XFLR5 using a batch analysis for the Reynolds numbers of 10000 to 70000 with a step size of 10000 to check the consistency of the airfoil over the expected Reynolds number range.

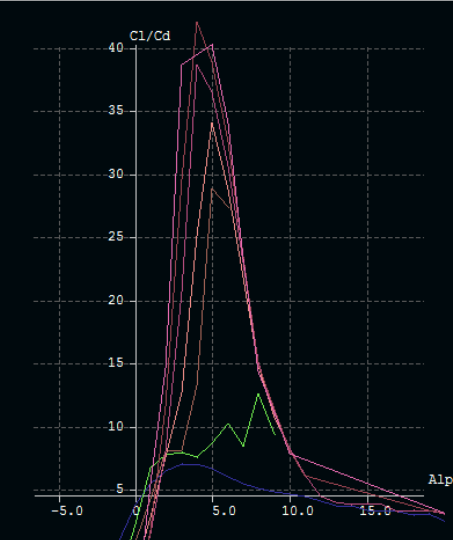
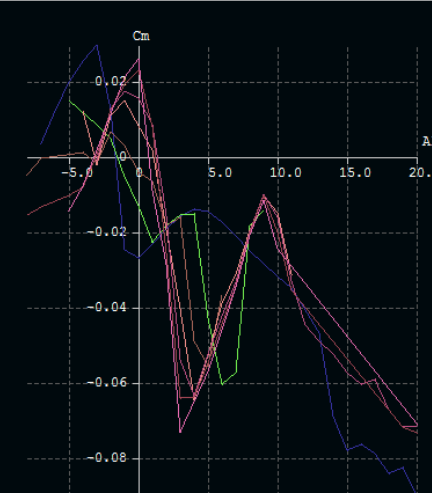
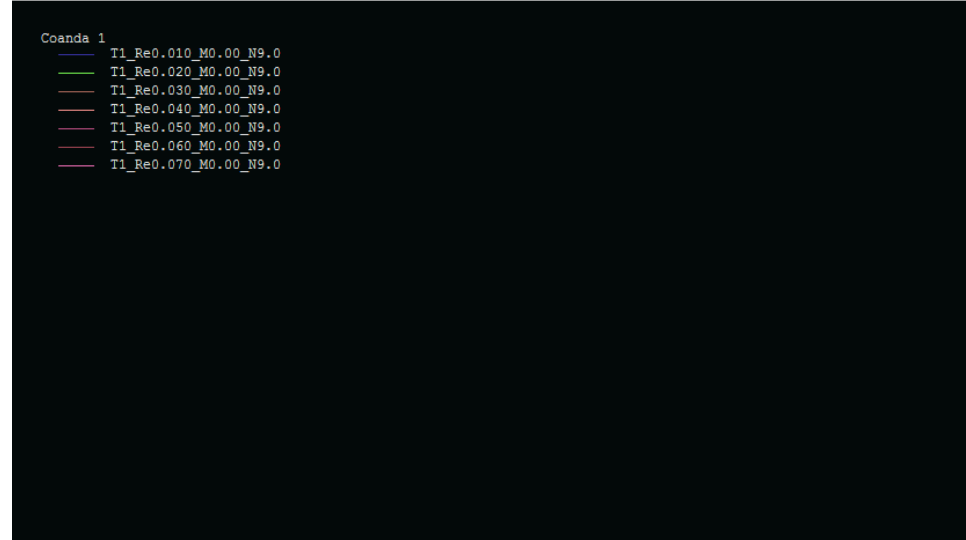
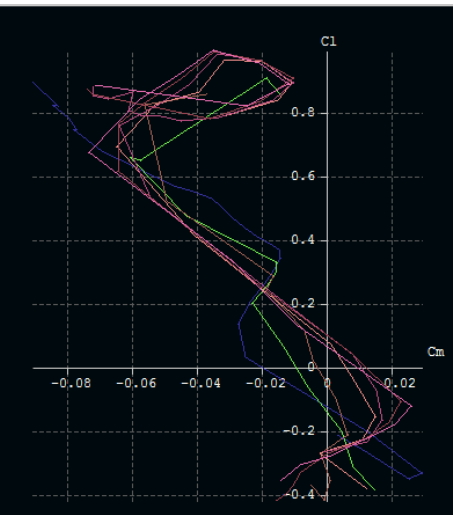
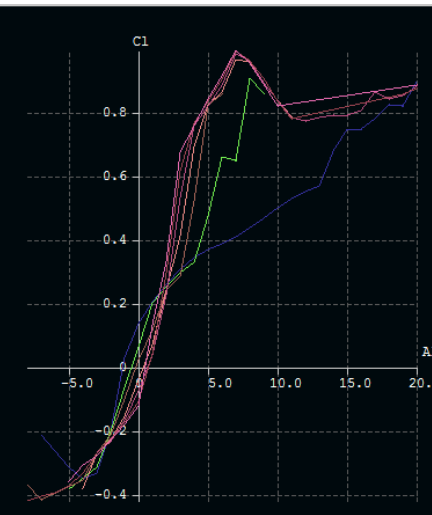
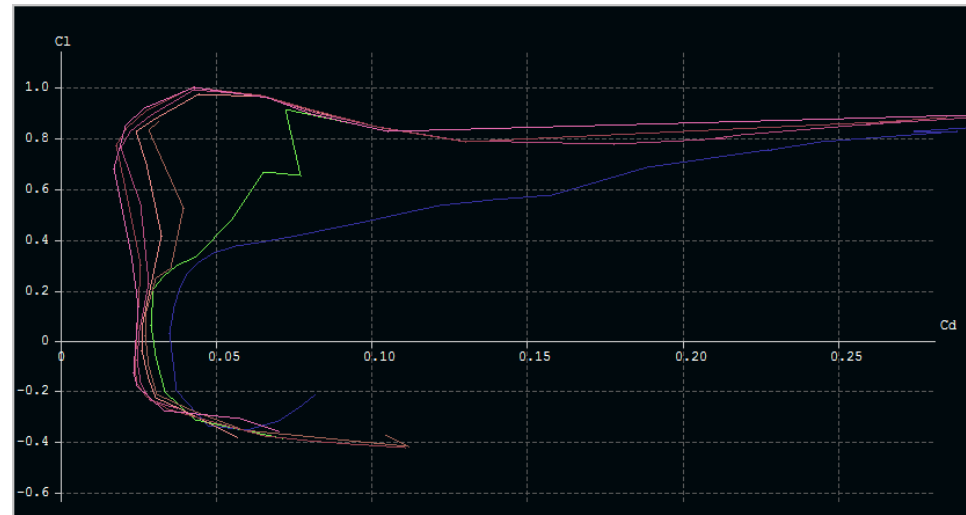


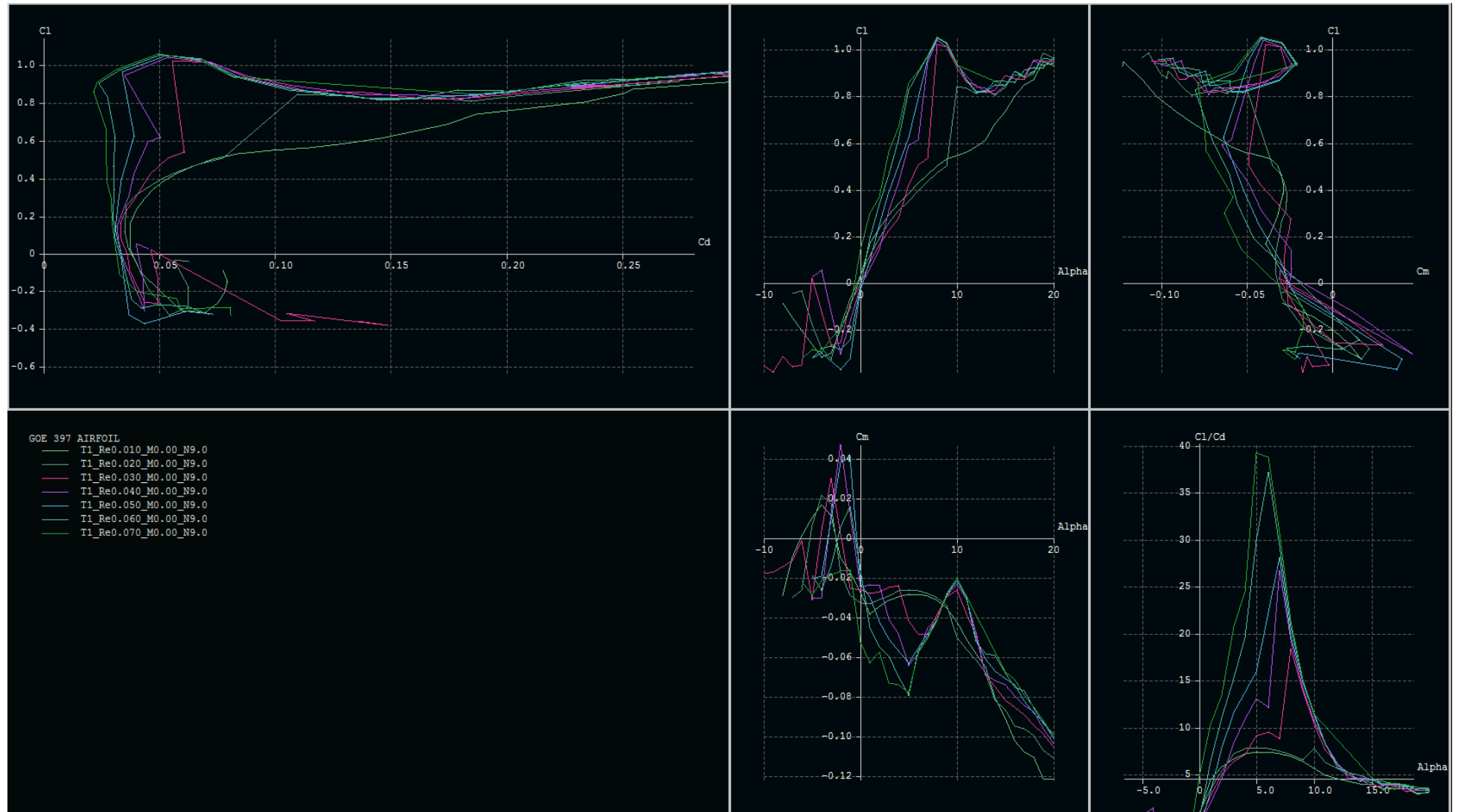


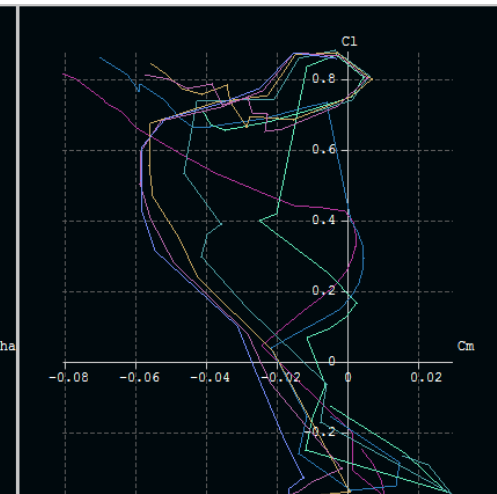
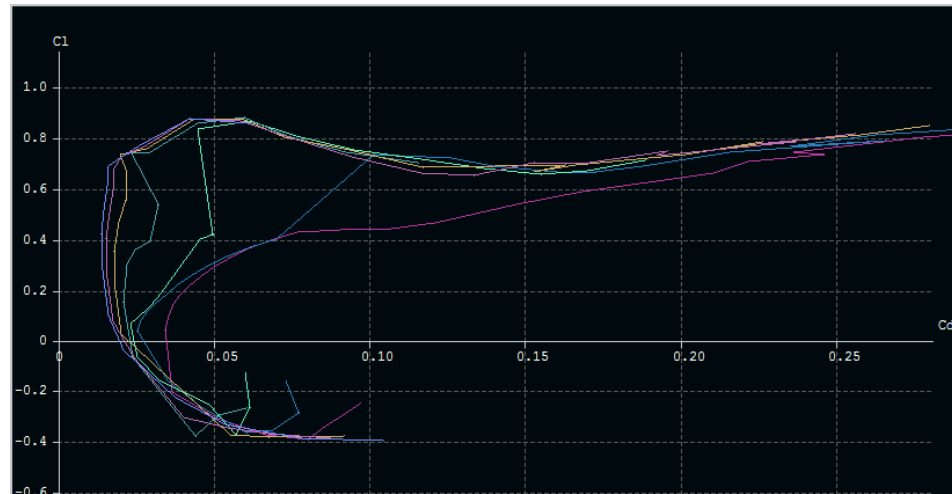






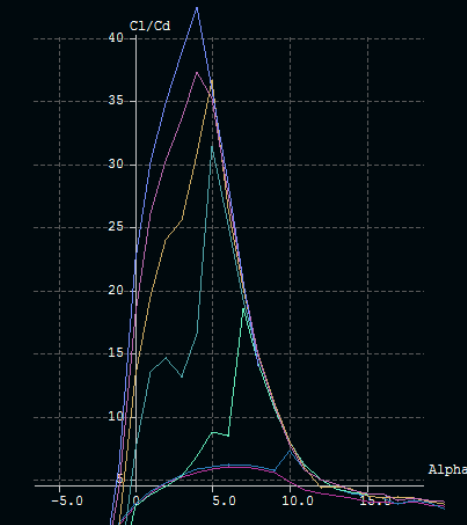
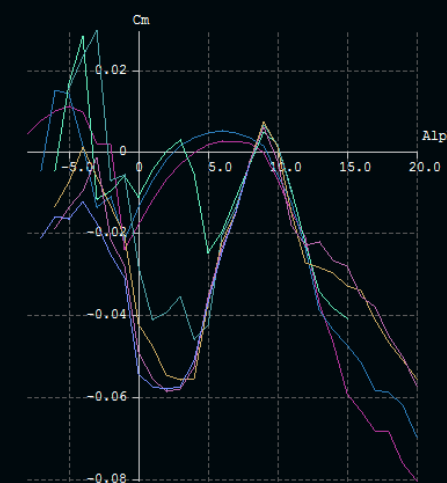


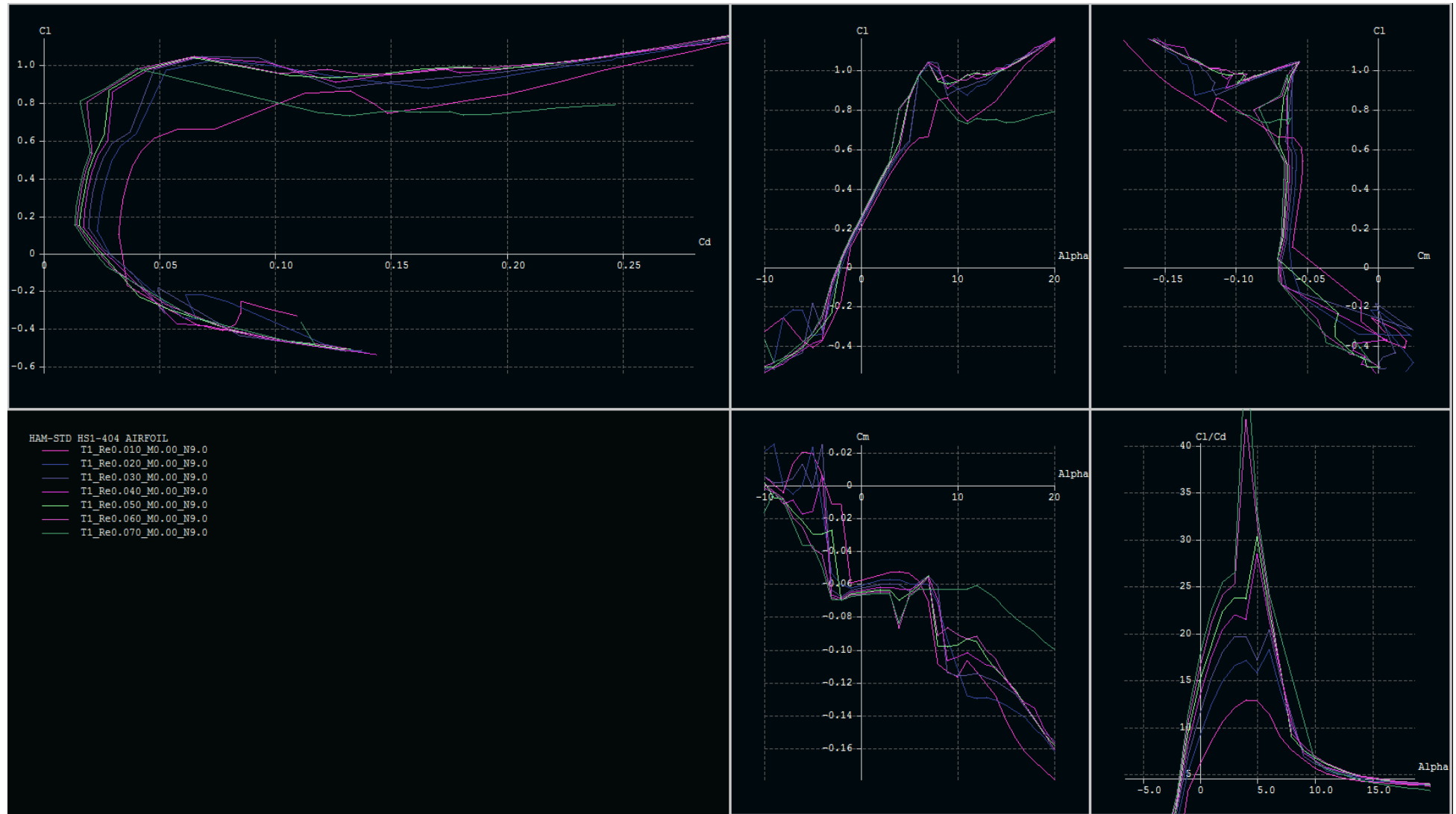




GOE 587 AIRFOIL

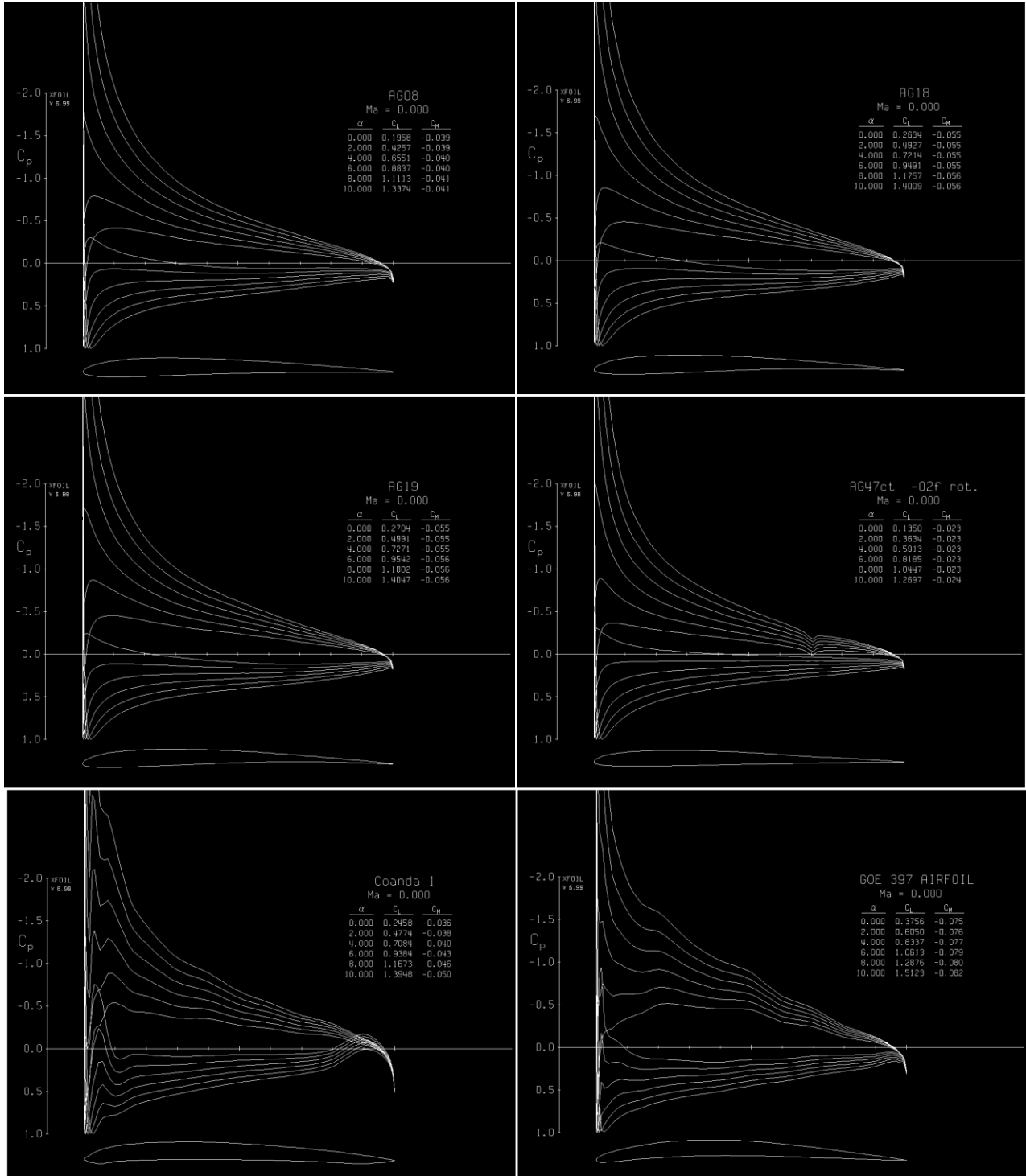
- T1\_Re0.010\_M0.00\_N9.0
- T1\_Re0.020\_M0.00\_N9.0
- T1\_Re0.030\_M0.00\_N9.0
- T1\_Re0.040\_M0.00\_N9.0
- T1\_Re0.050\_M0.00\_N9.0
- T1\_Re0.060\_M0.00\_N9.0
- T1\_Re0.070\_M0.00\_N9.0

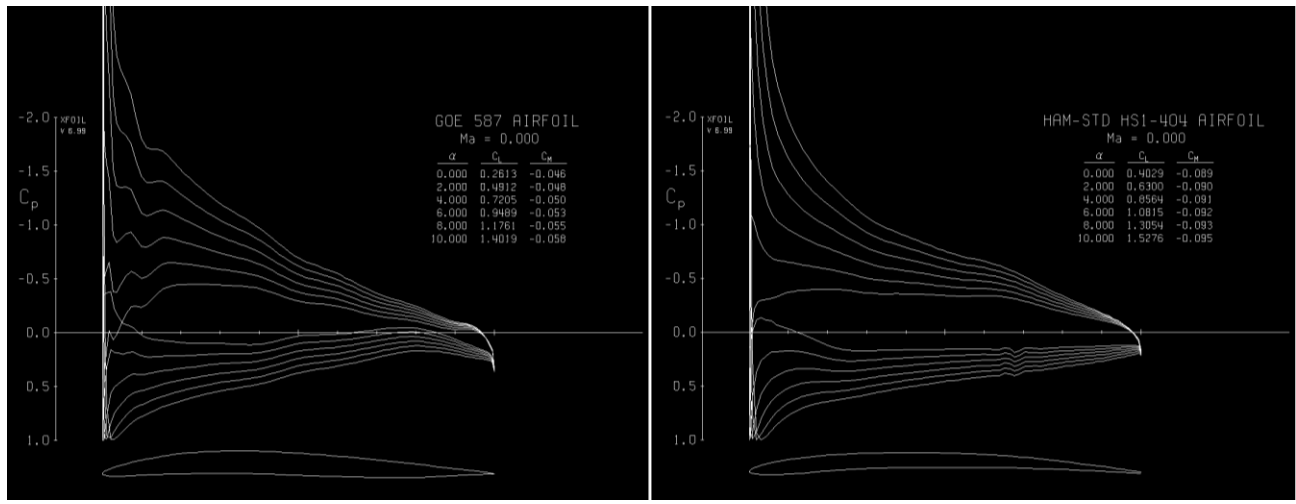




## Appendix F

Appendix F contains the pressure distributions created in XFOIL of the airfoils listed in Appendix D. The analysis was completed at a Reynolds number of 50000 and alpha value starting at 0 and ending at 10 with a step size of 2. This analysis was used to give an indication if early separation could occur.





## Appendix G

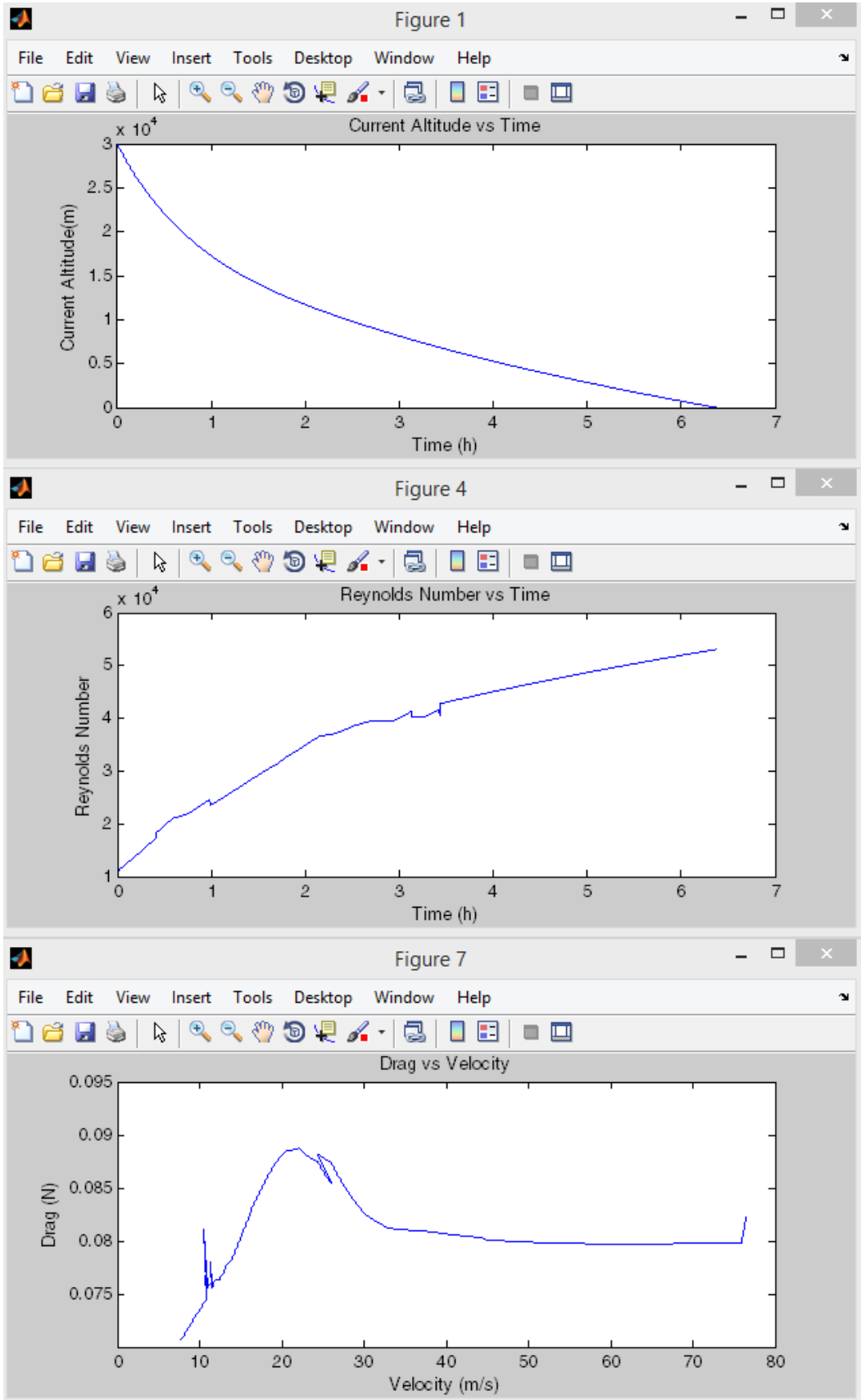
Appendix G contains the data from the MATLAB script varyingChordandLength.m. This was used to help determine the maximum distance possible for the aircraft to travel given ideal conditions.

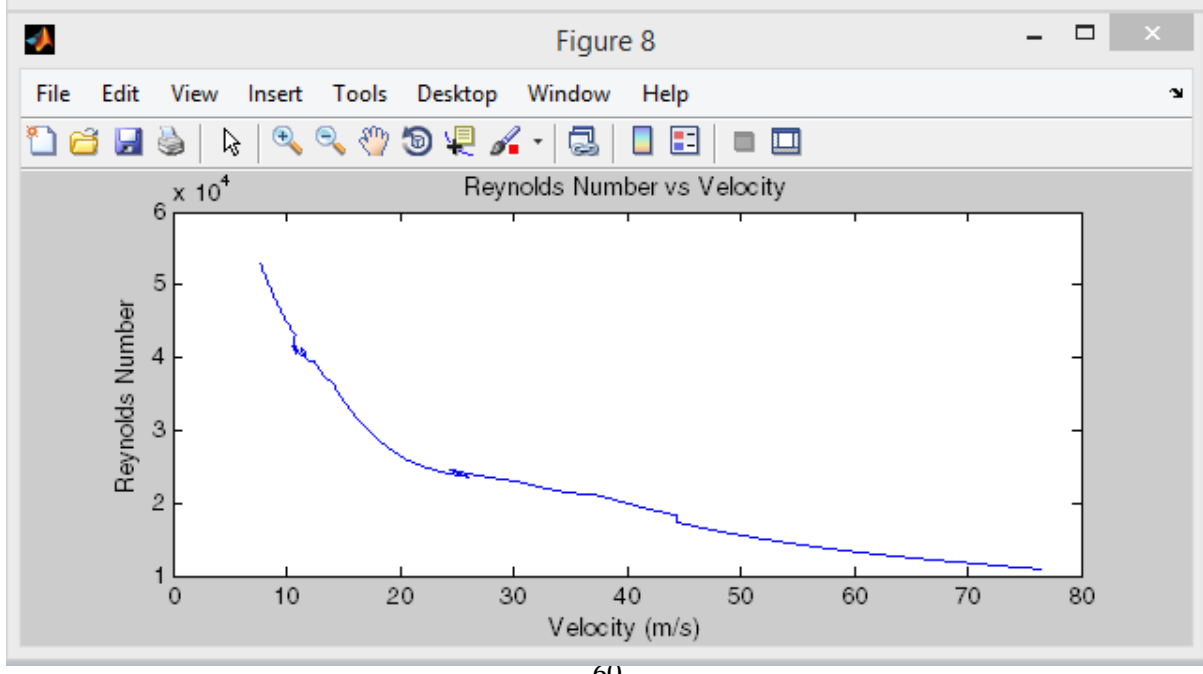
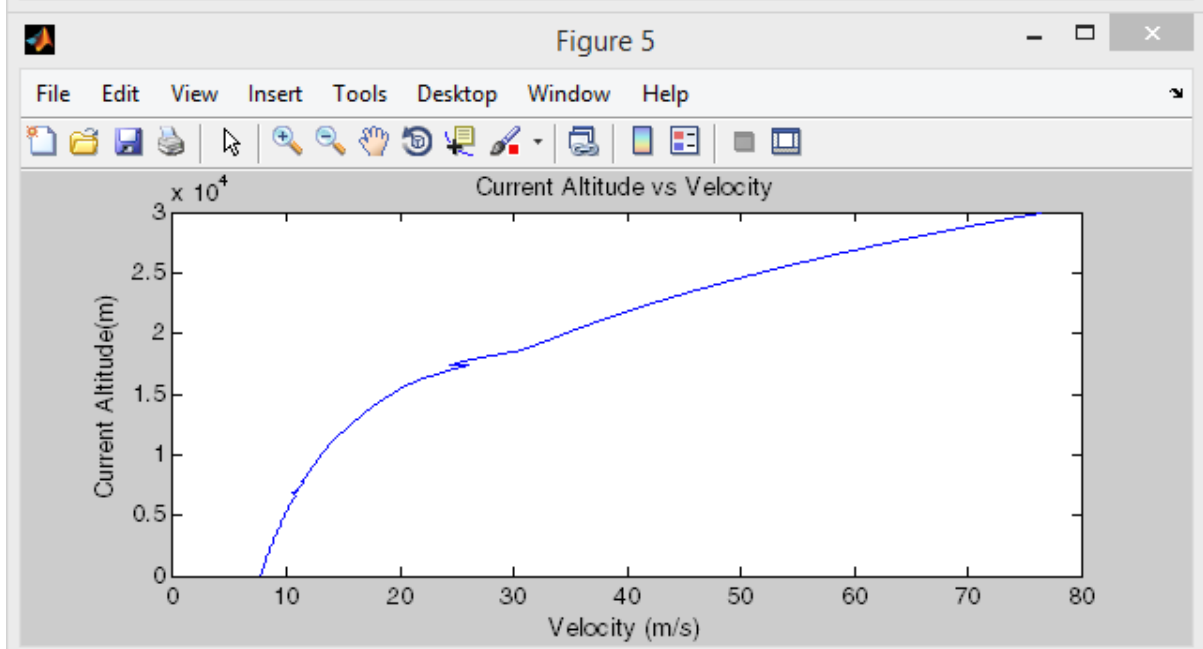
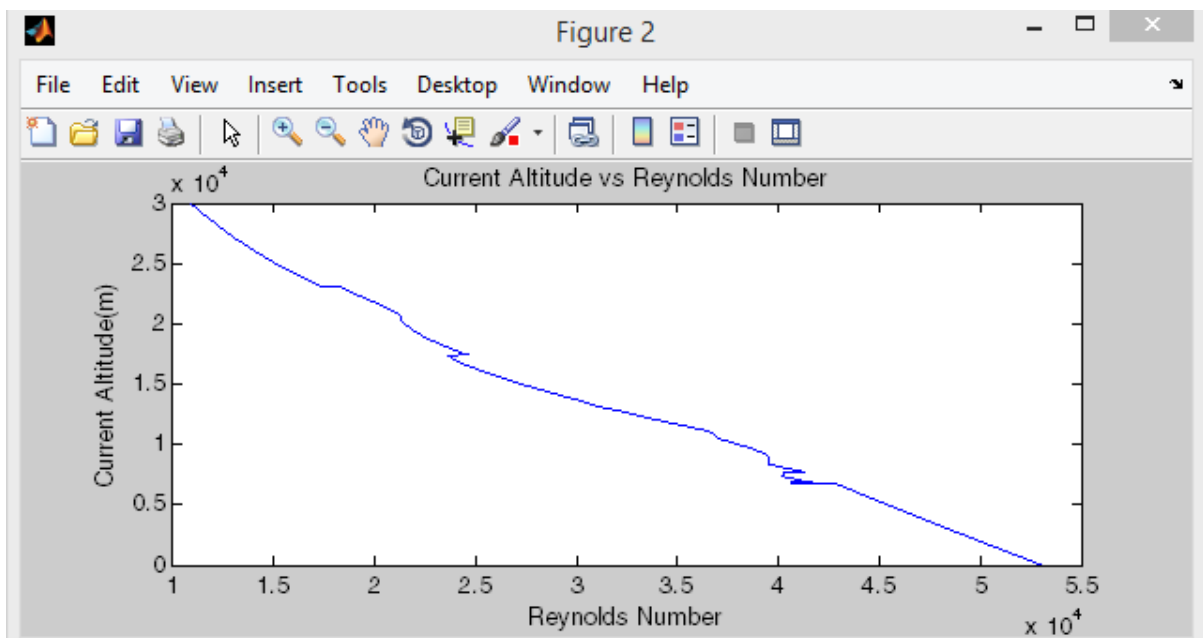
Span (m)	Chord Length(m)	Max Distance (m)	Mass (kg)	Max Allowable Mass (kg)	Safety Factor
0.1	0.05	238351.3877	0.053352031	0.104207748	1.953210516
0.1	0.06	207252.3492	0.054826924	0.180070988	3.284353263
0.1	0.07	182270.9796	0.05656998	0.285946059	5.054731461
0.1	0.08	162326.009	0.058581199	0.426834934	7.286210298
0.1	0.09	146589.0188	0.06086058	0.607739584	9.985767246
0.1	0.1	133377.146	0.063408123	0.833661981	13.14755806
0.1	0.11	121336.6978	0.066223829	1.109604096	16.75536001
0.1	0.12	111555.2689	0.069307697	1.440567903	20.78510696
0.1	0.13	103960.5512	0.072659728	1.831555372	25.20729734
0.1	0.14	96892.01959	0.076279921	2.287568475	29.98912995
0.1	0.15	89926.80997	0.080168277	2.813609185	35.09629103
0.2	0.05	369502.9186	0.056704062	0.052103874	0.918873752
0.2	0.06	332897.7813	0.059653849	0.090035494	1.509298996
0.2	0.07	305167.0856	0.063139961	0.14297303	2.264382621
0.2	0.08	280121.3274	0.067162398	0.213417467	3.177633237
0.2	0.09	257444.2633	0.07172116	0.303869792	4.236822076
0.2	0.1	238599.8013	0.076816246	0.41683099	5.426338963
0.2	0.11	220909.7783	0.082447658	0.554802048	6.729142602
0.2	0.12	205090.7063	0.088615395	0.720283951	8.128203387
0.2	0.13	191810.2597	0.095319456	0.915777686	9.607458137
0.2	0.14	180539.2077	0.102559843	1.143784238	11.15235951
0.2	0.15	169831.3612	0.110336554	1.406804592	12.75012259
0.3	0.05	444775.7758	0.060056092	0.034735916	0.578391209
0.3	0.06	413974.0622	0.064480773	0.060023663	0.930876908
0.3	0.07	386686.6618	0.069709941	0.095315353	1.367313638
0.3	0.08	362007.8855	0.075743596	0.142278311	1.878420329
0.3	0.09	340442.3444	0.082581739	0.202579861	2.453083007
0.3	0.1	320074.3954	0.090224369	0.277887327	3.079958647
0.3	0.11	300581.2377	0.098671487	0.369868032	3.748479354
0.3	0.12	283262.6558	0.107923092	0.480189301	4.449365671
0.3	0.13	267387.9049	0.117979184	0.610518457	5.174798082
0.3	0.14	252543.7748	0.128839764	0.762522825	5.918381098
0.3	0.15	239266.3768	0.140504831	0.937869728	6.674999852
0.4	0.05	490622.5914	0.063408123	0.026051937	0.410861189
0.4	0.06	466764.7162	0.069307697	0.045017747	0.649534593
0.4	0.07	444535.5637	0.076279921	0.071486515	0.937160311
0.4	0.08	422324.6141	0.084324795	0.106708734	1.265449067
0.4	0.09	402244.7771	0.093442319	0.151934896	1.625975228
0.4	0.1	384945.2855	0.103632493	0.208415495	2.011101826
0.4	0.11	366277.967	0.114895316	0.277401024	2.414380616

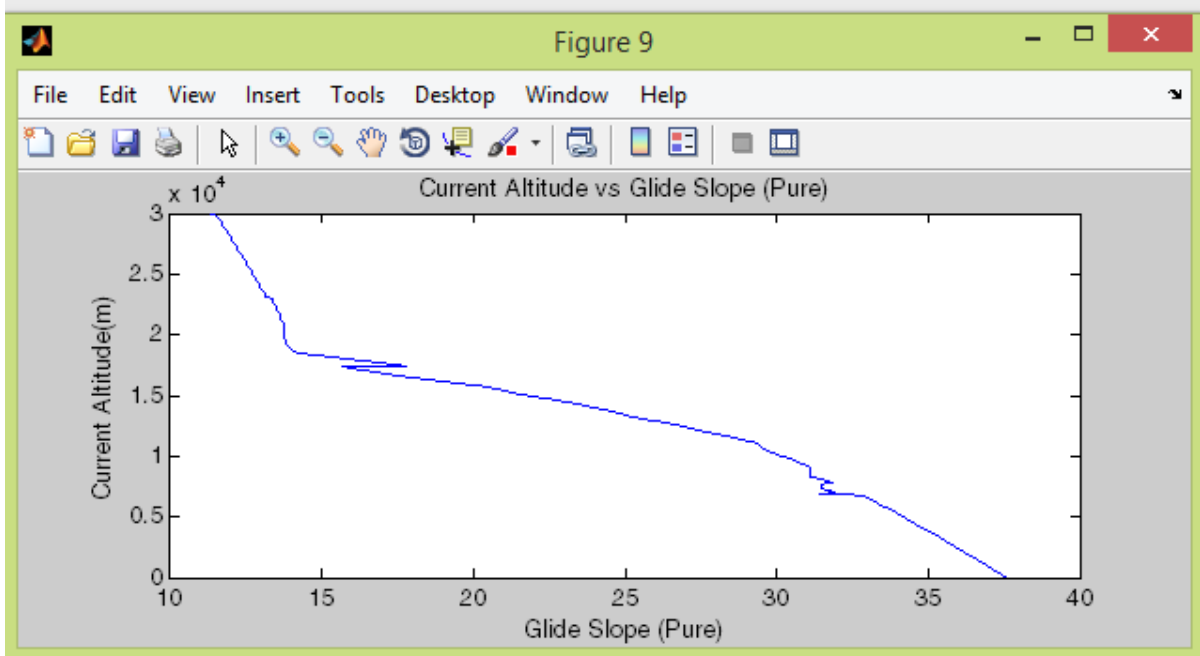
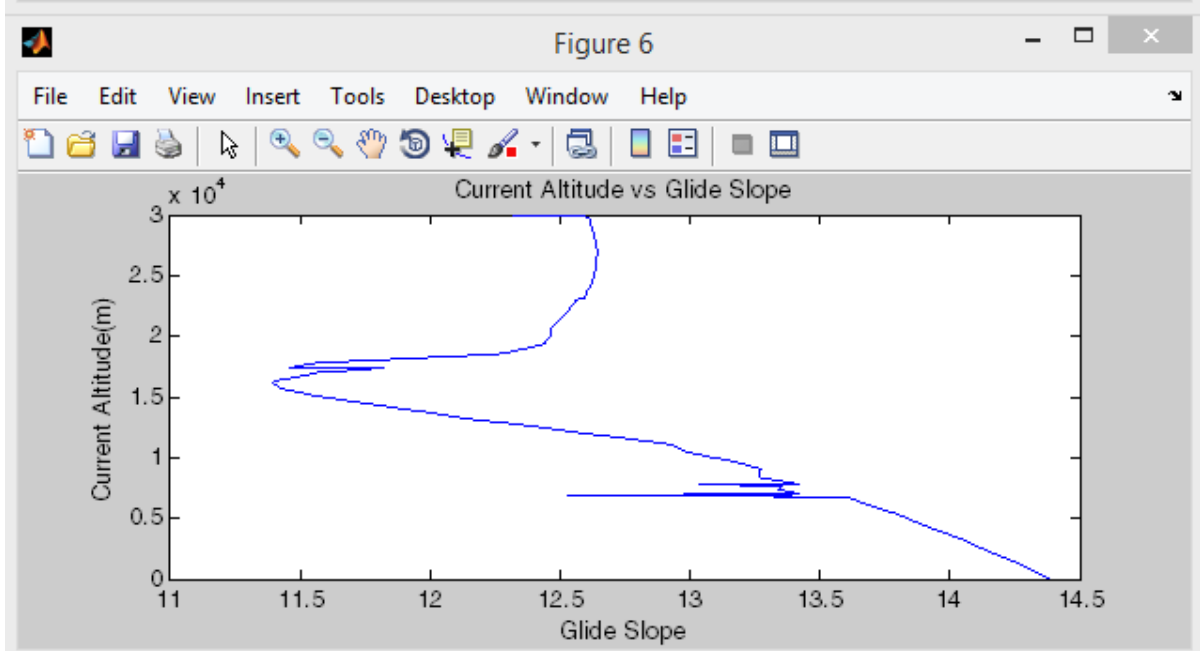
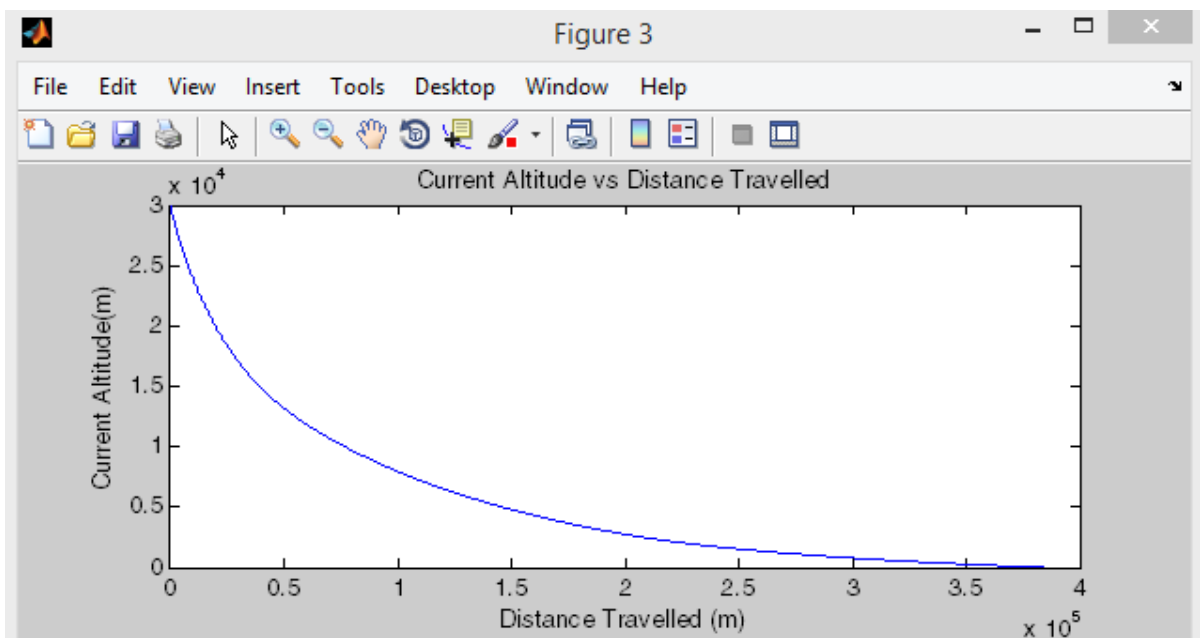
0.4	0.12	348225.9841	0.127230789	0.360141976	2.830619674
0.4	0.13	331018.8593	0.140638913	0.457888843	3.255776332
0.4	0.14	315529.8005	0.155119686	0.571892119	3.686779771
0.4	0.15	300355.6413	0.170673108	0.703402296	4.12134227
0.5	0.05	521882.7231	0.066760154	0.02084155	0.312185462
0.5	0.06	503181.2658	0.074134622	0.036014198	0.485794582
0.5	0.07	485961.8649	0.082849902	0.057189212	0.690274951
0.5	0.08	468616.6265	0.092905994	0.085366987	0.918853381
0.5	0.09	451006.229	0.104302899	0.121547917	1.165335942
0.5	0.1	436457.2507	0.117040616	0.166732396	1.424568685
0.5	0.11	420180.2303	0.131119145	0.221920819	1.692512707
0.5	0.12	403157.7718	0.146538487	0.288113581	1.966129083
0.5	0.13	386938.1017	0.163298641	0.366311074	2.243197327
0.5	0.14	371053.9004	0.181399607	0.457513695	2.522131678
0.5	0.15	355614.159	0.200841386	0.562721837	2.801822122

## Appendix H

Appendix H contains the plots from planeSim.m for a wing span of 400mm and a chord length of 100mm.



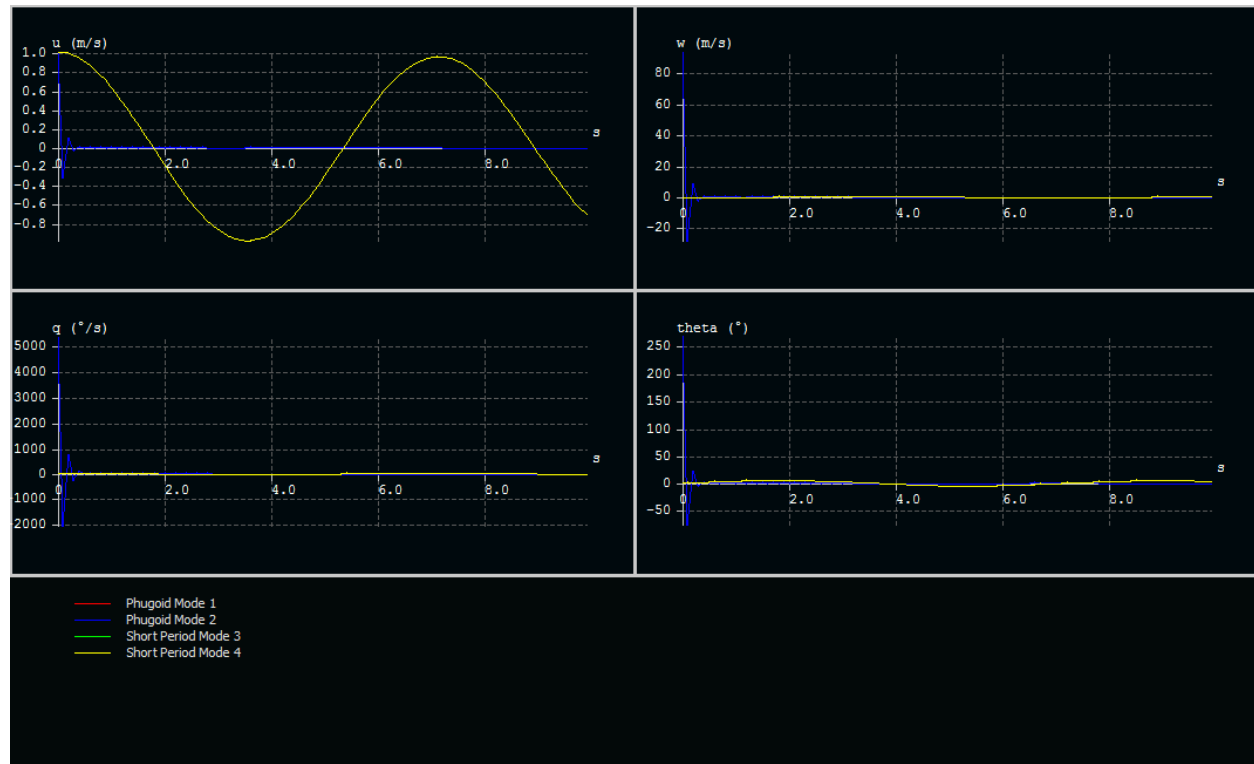




## Appendix I

Appendix I contains the stability results in graphical form from XFLR5.

### Longitudinal Modes

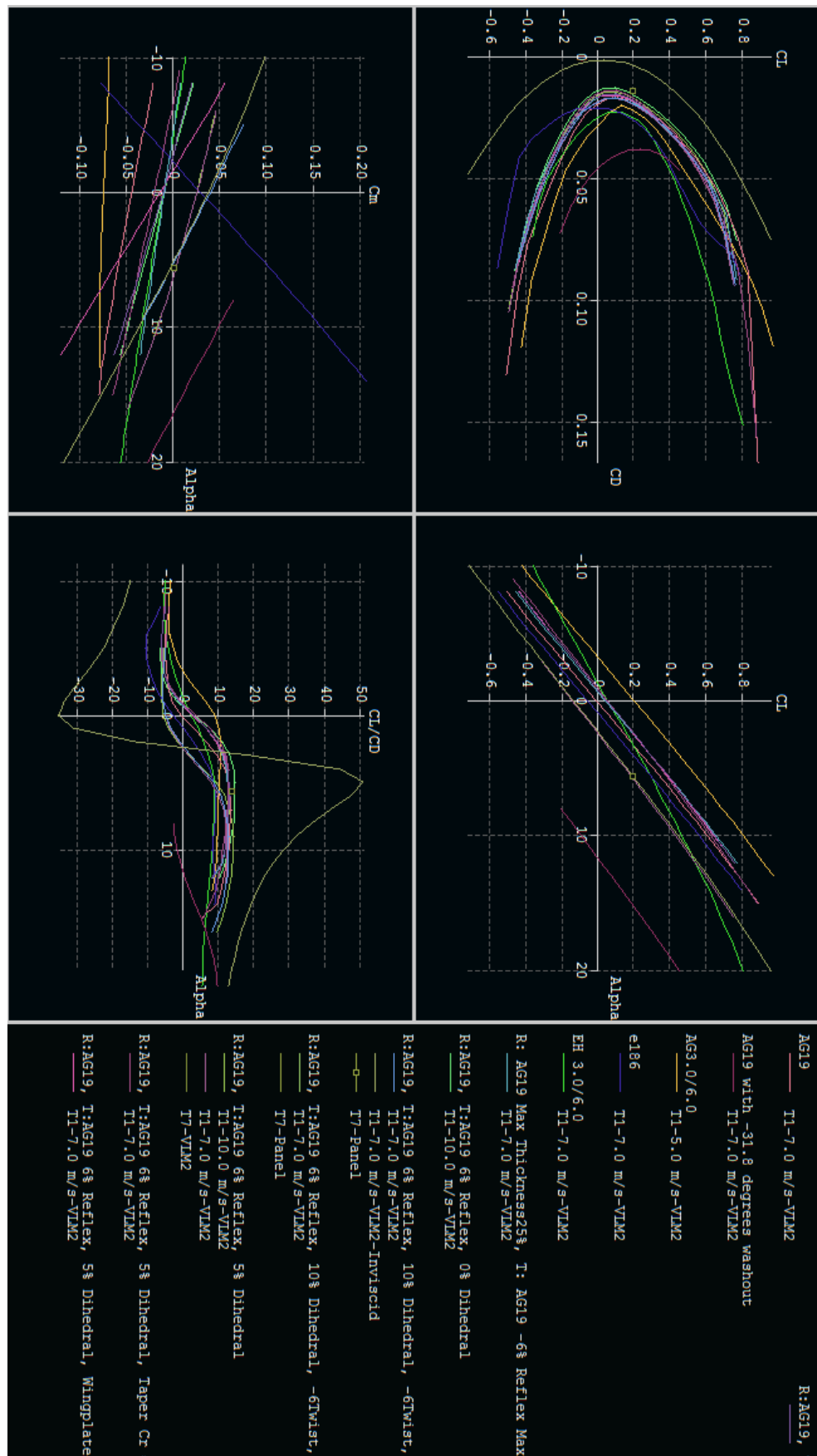


### Lateral Modes



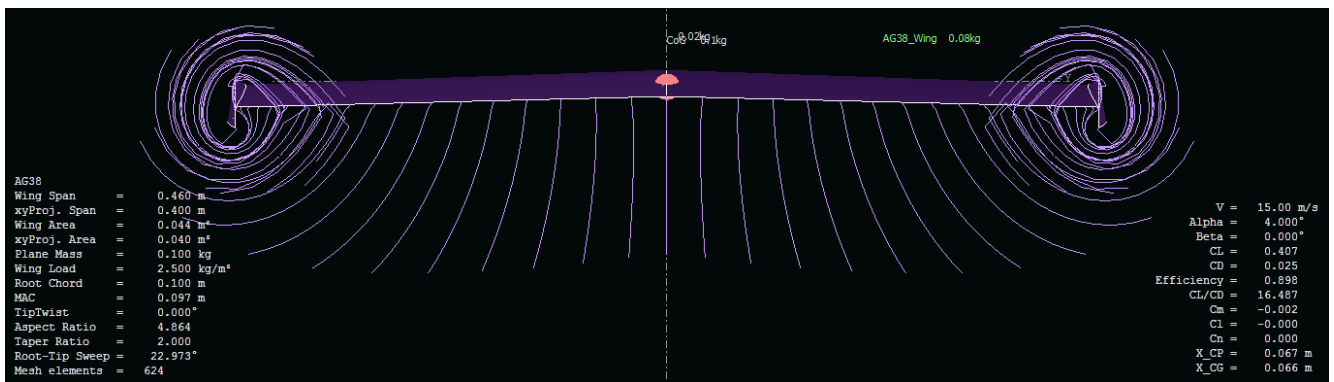
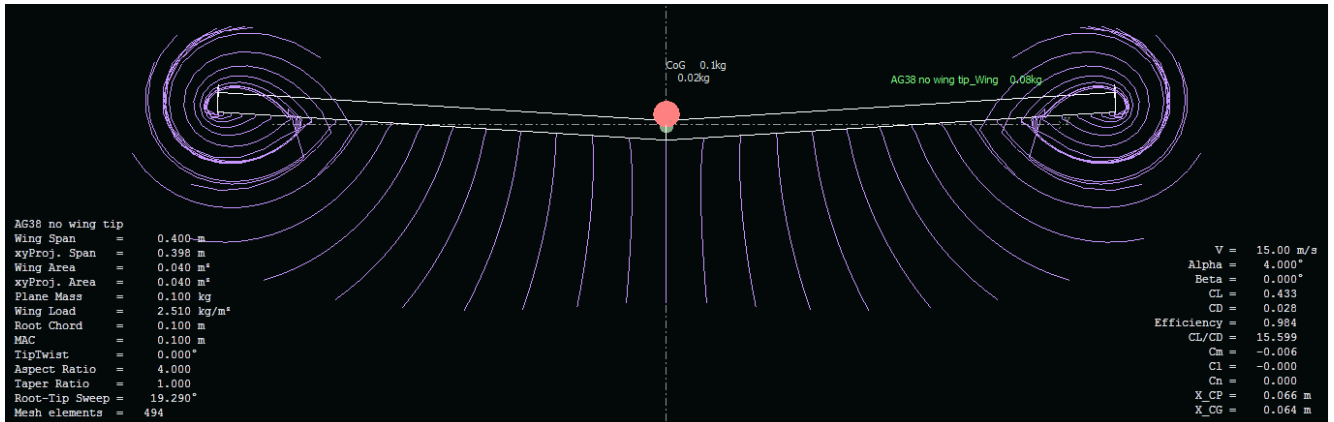
## Appendix J

Appendix J contains some of the designs tested for stability in XFLR5. The final design used was named R:AG19, T:AG19 6% Reflex, 10% Dihedral, -6Twist, 26degree Sweep.



## Appendix K

Appendix K contains the initial XFLR5 inviscid testing for wing tips on a AG38 airfoil. The results show a increase in glide slope from 15.999 to 16.487. These results could not be replicated in viscous testing.



## **Appendix H**

The following can be found on the attached Companion Disk:

- MATLAB code
- Python Code
- Beam bending data
- XFLR5 Analysis
- Airfoil profiles, data and images
- All CAD files for the moulds designed.

## Bibliography

- [1] C. A. Williams, “Packaging Systems Redesign: A Study in Designing More Sustainable Product Packaging Systems,” The Ohio State University, Ohio, 2010.
- [2] Airfoil Tools, “AG19 - Drela AG19 Airfoil,” 2014. [Online]. Available: <http://airfoiltools.com/airfoil/details?airfoil=ag19-il>. [Accessed 20 September 2014].
- [3] Wolfram Alpha, “Wolfram Alpha,” 2014. [Online]. Available: <http://www.wolframalpha.com/input/?i=distance+from+sydney+to+brisbane>. [Accessed 20 March 2014].
- [4] StratoStar, “Weather Balloon FAQ,” 2014. [Online]. Available: <http://www.stratostar.net/faq.html>. [Accessed 18 March 2014].
- [5] D. Windestål, “RCExplorer,” 2013. [Online]. Available: <http://rcexplorer.se/projects/2013/03/fpv-to-space-and-back/>. [Accessed 25 03 2014].
- [6] P. E. Pounds, *Paper Plane: Towards Disposable Low-Cost Folded Cellulose-Substrate UAVs*, Brisbane: The University of Queensland, 2012.
- [7] University of Sheffield, “3D printing trials of unmanned aircraft at the University of Sheffield broaden the possibilities for this emergent technology,” 2014 March 2014. [Online]. Available: <http://www.sheffield.ac.uk/news/nr/3d-printing-trials-of-unmanned-aircraft-1.364084>. [Accessed 4 April 2014].
- [8] J. Skurie, “Cheap, Disposable Drones Are the New Storm Chasers,” National Geographic, 25 July 2013. [Online]. Available: <http://news.nationalgeographic.com.au/news/2013/13/130725-drone-uav-uas-disposable-wildfire-storm-chasers/>. [Accessed 5 April 2014].
- [9] M. R. Reid, “Thin/Cambered/Reflexed Airfoil Development for Micro-Air Vehicles at Reynolds Numbers of 60,000 to 150,000,” Rochester Institute of Technology, New York, 2006.
- [10] T. J. Mueller, “Aerodynamic Measurements at Low Reynolds Numbers for Fixed Wing Micro-Air Vehicles,” University of Notre Dame, Belgium, 1999.
- [11] Keiding, “Types of Molded Fiber,” Keiding, 2013. [Online]. Available: <http://www.keiding.com/molded-fiber/types-of-molded-fiber/>. [Accessed 06 May 2014].
- [12] H. H. Schueneman and G. Schwinghammer, “Cushion Dynamics of Molded Pulp,” Westpak Inc., California .
- [13] J. Chen, Z. Qin, Z. Xu, L. Wu, Y. Wei, X. Wang and G. J. Duns, “Utilization of an Invasive Species (*Spartina alternifolia*) in the Molded Pulp Industry,” Nanjing University of Technology, Jiangsu, 2012.
- [14] R. H. Barnard and D. R. Philpott, Aircraft Flight, Fourth ed., Essex: Pearson, 2010.

- [15] M. Cavcar, “Minimum Drag Speed,” 2004. [Online]. Available: <http://home.anadolu.edu.tr/~mcavcar/htk224/MinDrag.pdf>. [Accessed 1 October 2014].
- [16] NASA, “Induced Drag Coefficient,” 2014. [Online]. Available: <http://www.grc.nasa.gov/WWW/k-12/airplane/induced.html>. [Accessed 1 October 2014].
- [17] Stanford, “Form Factor,” [Online]. Available: <http://adg.stanford.edu/aa241/drag/formfactor.html>. [Accessed 1 October 2014].
- [18] Federal Aviation Administration, Glider Flying Handbook, FAA-H-8083-13A ed., Oklahoma: United States Department of Transportation, 2013.
- [19] B. Beron-Rawdon, “Performance Analysis of a Family of R/C Thermal Sailplanes,” 1996. [Online]. Available: <http://www.rc-soar.com/tech/perfanal.htm>. [Accessed 20 03 2014].
- [20] NASA, “Reynolds Number,” 2014. [Online]. Available: <http://www.grc.nasa.gov/WWW/k-12/airplane/reynolds.html>. [Accessed 18 03 2014].
- [21] M. S. Selig, J. J. Guglielmo, A. P. Broeren and P. Giguere, Summary of Low-Speed Airfoil Data, First ed., Virginia: SoarTech Publications, 1995.
- [22] Tamkang University, “Airfoil Design,” [Online]. Available: <http://mail.tku.edu.tw/095980/airfoil%20design.pdf>. [Accessed 06 July 2014].
- [23] A. Deperrois, “About Stability Analysis using XFLR5,” XFLR5, 2010.
- [24] M. Hepperle, “Basic Design of Flying Wing Models,” 1 December 2002. [Online]. Available: <http://www.mh-aerotools.de/airfoils/flywing1.htm>. [Accessed 1 May 2014].
- [25] California Institute of Technology, “Cantilever Beam Experiment,” March 2003. [Online]. Available: <http://www.rpgroup.caltech.edu/courses/me96/beam.pdf>. [Accessed 14 May 2014].
- [26] FlashForge USA, “FlashForge Creator X,” 2014. [Online]. Available: <http://www.flashforge-usa.com/shop/3d-printers/creator-x-dual-extruder.html>. [Accessed 30 July 2014].
- [27] 3M, “3MTM Water Activated Paper Tape 6141 Natural Light Duty, 1-1/2 in x 500 ft, 20 rolls per case Bulk,” 3M, 2014. [Online]. Available: [http://solutions.3m.com/wps/portal/3M/en\\_US/Adhesives/Tapes/Products/~/3M-Water-Activated-Paper-Tape-6141?N=5393837+4294864995&rt=rud](http://solutions.3m.com/wps/portal/3M/en_US/Adhesives/Tapes/Products/~/3M-Water-Activated-Paper-Tape-6141?N=5393837+4294864995&rt=rud). [Accessed 8 September 2014].
- [28] C. Reyes, RCadvisor's Model Airplane Design Made Easy, Albuquerque: RCadvisor.com, 2009.
- [29] M. S. Genç, I. Karasu, H. H. Açıkel and M. T. Akpolat, “Low Reynolds Number Flows and Transition,” InTech, Rijeka, 2012.
- [30] M. Hepperle, “Reflex and Lift & Drag,” 3 September 2003. [Online]. Available: [http://www.mh-aerotools.de/airfoils/nf\\_4.htm](http://www.mh-aerotools.de/airfoils/nf_4.htm). [Accessed 1 May 2014].
- [31] Airfoil Tools, “Airfoil Tools,” 2014. [Online]. Available: <http://airfoiltools.com/>. [Accessed 22 March 2014].

- [32] “The Panknin Twist Formula,” [Online]. Available: <http://www.b2streamlines.com/Panknin.html>. [Accessed 13 July 2014].
- [33] Soaring Society of America, “Glider Lift Sources,” 2013. [Online]. Available: <http://www.ssa.org/GliderLiftSources>. [Accessed 15 03 2014].
- [34] E. Ibanez, “DIY Drones,” 2011. [Online]. Available: <http://diydrones.com/forum/topics/multiplex-funjet-in-wind-tunnel>. [Accessed 25 03 2014].
- [35] The University of Queensland, *PF388 Risk Assessment Form*, Brisbane: The University of Queensland, 2007.
- [36] Multiplex, “Multiplex,” 2014. [Online]. Available: <http://www.multiplex-rc.de/en/products>. [Accessed 26 03 2014].
- [37] M. Drela and H. Youngren, “XFOIL Subsonic Airfoil Development System,” 2013. [Online]. Available: <http://web.mit.edu/drela/Public/web/xfoil/>. [Accessed 02 June 2014].
- [38] “XFLR5,” 2014. [Online]. Available: <http://www.xflr5.com/xflr5.htm>. [Accessed 04 July 2014].
- [39] Python Software Foundation, “Python,” 2014. [Online]. Available: <https://www.python.org/>. [Accessed 25 March 2014].
- [40] MathWorks, “MATLAB,” 2014. [Online]. Available: <http://www.mathworks.com.au/products/matlab/>. [Accessed 25 March 2014].
- [41] Granta Design, “CES EduPack 2014,” Granta Design, 2014. [Online]. Available: <http://www.grantadesign.com/education/edupack/edupack2014.htm>. [Accessed 10 August 2014].